Frontiers in Bioscience Landmark

Front. Biosci. (Landmark Ed) **2026**; 31(3): 47686
https://doi.org/10.31083/FBL47686

Original Research

ASS1 Promotes Atherosclerotic Inflammation Through the NLRP3/IL-33/ST2 Axis in Ox-LDL–Induced Foam Cells

Shaoyu Wu[1,2,3,4,†], Feihuang Han[1,2,5,†], Zheng Qiao[3,4,6], Sheng Yuan[3,4,6], Xiaohui Bian[3,4,6], Bin Zhang[1,2,5], Kefei Dou[3,4,6,*], Dunliang Ma[1,2,5,*]

[1]Department of Cardiology, Guangdong Provincial People's Hospital, Guangdong Academy of Medical Sciences, Southern Medical University, 510080 Guangzhou, Guangdong, China
[2]Guangdong Provincial Key Laboratory of Clinical Pharmacology, Guangdong Provincial People's Hospital, Guangdong Academy of Medical Sciences, Southern Medical University, 510080 Guangzhou, Guangdong, China
[3]Department of Cardiology, Fuwai Hospital, National Center for Cardiovascular Diseases, Chinese Academy of Medical Sciences and Peking Union Medical College, 100037 Beijing, China
[4]Coronary Heart Disease Center, State Key Laboratory of Cardiovascular Disease, Fuwai Hospital, National Center for Cardiovascular Diseases, Chinese Academy of Medical Sciences and Peking Union Medical College, 100037 Beijing, China
[5]Medical Research Institute, Guangdong Provincial People's Hospital, Guangdong Academy of Medical Sciences, Southern Medical University, 510080 Guangzhou, Guangdong, China
[6]Cardiometabolic Medicine Center, National Clinical Research Center for Cardiovascular Diseases, Fuwai Hospital, National Center for Cardiovascular Diseases, Chinese Academy of Medical Sciences and Peking Union Medical College, 100037 Beijing, China
*Correspondence: drdoukefei@126.com (Kefei Dou); Drmadunliang@163.com (Dunliang Ma)
[†]These authors contributed equally.
Academic Editor: Paramjit S. Tappia
Submitted: 26 October 2025 Revised: 22 January 2026 Accepted: 6 February 2026 Published: 16 March 2026

Abstract

Background: Atherosclerosis is a chronic inflammatory disease characterized by lipid-driven immune dysregulation. Argininosuccinate synthase 1 (ASS1) has been implicated in macrophage inflammation, yet its precise mechanistic role in foam cell-mediated vascular injury during atherosclerosis remains unclear. This study investigates whether ASS1 promotes disease progression via the NLRP3/IL-33/ST2 axis. **Methods**: An *in vitro* foam cell model was established using phorbol 12-myristate 13-acetate (PMA)-differentiated U937 macrophages treated with oxidized low-density lipoprotein (ox-LDL). The role of ASS1 was assessed via knockdown (si-ASS1) and overexpression (ASS1 overexpression) plasmids. Co-culture systems with human umbilical vein endothelial cells (HUVECs) and human aortic vascular smooth muscle cells (HAVSMCs) were used to evaluate endothelial apoptosis and VSMC proliferation/migration. *In vivo*, atherosclerosis was induced in apolipoprotein E-deficient (ApoE)-deficient mice via a 12-week high-fat diet, and ASS1 expression was modulated using AAV9 vectors. Molecular analyses included ROS detection, enzyme-linked immunosorbent assay (ELISA), qPCR, western blot, and immunofluorescence. Plaque burden was assessed via Oil Red O staining. **Results**: Ox-LDL treatment significantly upregulated ASS1 expression in U937-derived foam cells. ASS1 overexpression enhanced intracellular ROS production, NLRP3 inflammasome activation, STAT3 phosphorylation, and IL-33 secretion. These effects were reversed by ASS1 knockdown. Rescue experiments demonstrated that STAT3 is required for ASS1-mediated NLRP3 activation and IL-33 upregulation. ASS1 altered IL-33 receptor ST2 signaling by increasing the soluble decoy isoform (sST2) and decreasing the membrane-bound signaling isoform (ST2L). In co-culture, ASS1-overexpressing foam cells promoted HUVEC apoptosis (via mitochondrial pathway) and HAVSMC proliferation, migration, and dedifferentiation. NLRP3 overexpression alone mimicked the pro-inflammatory effects of ASS1 and reversed the anti-inflammatory effects of ASS1 knockdown. *In vivo*, ASS1 knockdown in ApoE$^{-/-}$ mice reduced plaque lipid deposition, serum levels of IL-33 and IL-1β, and vascular expression of NLRP3 and p-STAT3, while ASS1 overexpression exacerbated these parameters. **Conclusions**: ASS1 drives atherosclerosis by activating the STAT3/NLRP3 inflammasome axis, shifting the IL-33/ST2 balance toward a pro-inflammatory state, and amplifying foam cell–mediated endothelial injury and smooth muscle cell dysfunction. Targeting ASS1 may offer a novel therapeutic strategy for inflammatory vascular disease.

Keywords: atherosclerosis; ASS1; NLRP3 inflammasome; IL-33; ST2; foam cells; endothelial cells; vascular smooth muscle cells

1. Introduction

Atherosclerosis (AS) is a chronic inflammatory disease characterized by the gradual accumulation of cholesterol within arterial walls, which triggers a persistent and unresolved immune response [1]. The onset of AS involves endothelial dysfunction, initiating a cascade of events that includes the release of low-density lipoproteins (LDLs), infiltration of macrophages, and activation of vascular smooth muscle cells (VSMCs). These processes lead to foam cell formation and extracellular matrix remodeling, thereby driving disease progression [2]. Foam cells—a hallmark of all AS stages—originate from monocytes that infiltrate developing atheromas and subsequently internalize modified LDL [3]. Reactive oxygen species (ROS) produced by foam cells initiate inflammatory responses that recruit additional macrophages into the vascular intima, further promoting the development of fatty streaks and exacerbating AS [4,5]. A deeper understanding of the mechanisms regulating foam cell-mediated inflammation may therefore reveal novel therapeutic targets for AS.

The pyrin domain-containing protein 3 (NLRP3) inflammasome—composed of NLRP3, caspase-1, and apoptosis-associated speck-like protein containing a CARD (ASC)—represents a form of inflammatory cell death implicated in the pathogenesis of AS. Activation of the NLRP3 inflammasome can be triggered by specific molecules, including lipopolysaccharide as a pathogen-associated molecular pattern (PAMP), as well as oxidized LDL (ox-LDL) and cholesterol crystals acting as damage-associated molecular patterns (DAMPs) [6,7]. At the molecular level, dysregulated NLRP3 inflammasome activation elevates the levels of pro-inflammatory cytokines, namely interleukin (IL)-1β, IL-18, and IL-33. These cytokines are associated with macrophage recruitment to aortic lesions, thereby contributing to foam cell formation and the development of atherosclerotic plaques [8]. Soluble suppression of tumorigenicity 2 (sST2), a member of the IL-1 family, acts as a decoy receptor for IL-33 and is involved in cardiac remodeling and inflammatory processes [9]. The IL-33/ST2 signaling pathway, predominantly expressed in arterial endothelium, plays a critical role in AS-related inflammation. The balance between its two isoforms—the protective membrane-bound signaling receptor (ST2L) and the deleterious soluble decoy receptor (sST2)—is a key determinant of disease outcome [10,11]. McLaren *et al.* [10] demonstrated the importance of ST2 in mediating IL-33-driven macrophage foam cell formation [12], and several studies have reported the activation of both NLRP3 and IL-33/ST2 pathways in macrophages during cardiovascular disease [13,14].

In recent years, argininosuccinate synthase 1 (ASS1) has gained attention for its role in catalyzing the penultimate step of arginine biosynthesis. Together with argininosuccinate lyase (ASL), ASS1 facilitates arginine synthesis from aspartate, citrulline, and ATP in various tissues and cells [15,16]. ASS1 is known to regulate inflammatory macrophage activation and antibacterial defense by depleting cellular citrulline [17]. Elevated arginase levels and activity have been observed in several cardiovascular disorders, including AS [18–20]. Moreover, a recent study linked ASS1 expression to the anti-inflammatory effects of canagliflozin, which subsequently inhibited AS progression [19]. During early AS, ox-LDL accumulation induces macrophage dysfunction and foam cell formation [21]. Emerging evidence indicates that ox-LDL upregulates ASS1 expression in macrophages, promoting ROS generation and pro-inflammatory cytokine secretion [17,22]. ASS1 has also been shown to regulate NLRP3 inflammasome activation and influence IL-33 expression. Nevertheless, the precise mechanistic relationship between ASS1 and the NLRP3/IL-33/ST2 axis in foam cell-driven endothelial injury and VSMC dysfunction remains poorly understood.

This study investigates the hypothesis that ASS1 exacerbates AS by activating the STAT3/NLRP3 inflammasome axis, disrupting the IL-33/ST2 balance, and amplifying foam cell-mediated inflammation. We used PMA-differentiated U937 macrophages exposed to ox-LDL to generate foam cells and examined the role of ASS1 in regulating ROS, NLRP3 activation, and IL-33 secretion. Co-culture systems with human umbilical vein endothelial cells (HUVECs) and human aortic vascular smooth muscle cells (HAVSMCs) were employed to assess the effects of ASS1 on endothelial apoptosis and smooth muscle cell proliferation/migration. Furthermore, an *in vivo* atherosclerosis model was established using apolipoprotein E-deficient (ApoE$^{-/-}$) mice fed a high-fat diet for 12 weeks, with ASS1 expression modulated via AAV9 vectors. Lipid accumulation was evaluated by Oil Red O staining, and key inflammatory markers—including NLRP3, phosphorylated STAT3 (p-STAT3), IL-33, and IL-1β—were analyzed. Our findings aim to elucidate the functional role of ASS1 in integrating the NLRP3 inflammasome and IL-33/ST2 pathways, providing new insights into foam cell-driven inflammatory signaling in atherosclerosis.

2. Experimental Section

2.1 Construction of Monocyte-Derived Foam Cell

The U937 human monocytic cell line (PCS-100-011) was procured from the American Type Culture Collection (ATCC, Rockville, MD, USA). Cells were maintained in Dulbecco's Modified Eagle Medium (DMEM; Thermo Fisher Scientific, Waltham, MA, USA) supplemented with 10% fetal bovine serum (FBS), and incubated at 37 °C under a humidified atmosphere containing 5% CO_2. To differentiate U937 cells into foam cells, they were first stimulated with 100 nM phorbol 12-myristate 13-acetate (PMA) for 48 h, followed by treatment with 50 µg/mL oxidized low-density lipoprotein (ox-LDL; Sigma-Aldrich, St. Louis, MO, USA) for an additional 48 h.

2.2 Cell Transfection

Small interfering RNA targeting ASS1 (si-ASS1: 5′-UCAAUGAACACCUUUUUGGCC-3′), ASS1 overexpression plasmid (pCDNA3.0-ASS1), NLRP3 overexpression plasmid (pCDNA3.0-NLRP3), and their corresponding negative controls (scrambled siRNA [si-NC] for knockdown and empty vectors for overexpression) were commercially obtained from GenePharma (Shanghai, China). Foam cells were transfected with the indicated plasmids or siRNAs, either alone or in combination with their respective controls, using Lipofectamine 2000 (Life Technologies, Carlsbad, CA, USA). To further investigate the functional link between ASS1 and STAT3 signaling, we performed rescue experiments using STAT3-specific small interfering RNA (si-STAT3) and a constitutively active STAT3 mutant plasmid (STAT3-CA). The si-STAT3 (target sequence: 5′-GAACCAUGUGGAUAUCAUA-3′) and STAT3-CA overexpression plasmid (pCDNA3.1-STAT3-CA) were purchased from GenePharma (Shanghai, China). U937 foam cells were co-transfected with either si-STAT3 or STAT3-CA along with ASS1 overexpression or knockdown (si-ASS1) plasmids using Lipofectamine 2000 according to the manufacturer's instructions. Cells were harvested 48 hours post-transfection for subsequent analyses.

2.3 ROS Detection

Intracellular reactive oxygen species (ROS) levels were measured using the fluorescent probe 2′,7′-dichlorofluorescin diacetate (DCFH-DA; Sigma-Aldrich). Cells were incubated with 10 µM DCFH-DA for 30 min at 37 °C, washed thoroughly, and analyzed immediately on a FACScan flow cytometer (Becton-Dickinson, Mountain View, CA, USA). Data were processed with CellQuest software (version 4.1; BD Biosciences, Franklin Lakes, NJ, USA) and presented as fluorescence intensity histograms.

2.4 Quantitative Real-Time PCR

Total RNA was isolated from foam cells using Trizol reagent from Invitrogen (Carlsbad, CA, USA). Subsequently, cDNA synthesis was performed using the M-MLV reverse transcriptase kit from TaKaRa Co. (Dalian, Shandong, China). Quantitative real-time PCR amplification was conducted on an ABI 7500 Real-Time PCR System by Applied Biosystems. The amplification reaction was performed using the 1× FastStart Essential DNA Green Master from Roche (Mannheim, Germany), and the PCR protocol included an initial step at 50 °C for 2 minutes, followed by denaturation at 95 °C for 5 minutes, and 40 amplification cycles (4 seconds at 95 °C and 30 seconds at 60 °C). The relative quantity of target genes was determined using the $2^{-\Delta\Delta Ct}$ method, with normalization to GAPDH as the internal control. The primer sequences used were as follows:

ASS1 forward: 5′-TGAAATTTGCTGAGCTGGTG-3′ and ASS1 reverse: 5′-ATGTACACCTGGCCCTTGAG-3′; ST2L (membrane-bound isoform) forward: 5′-CCTGGTGAAGTTCAACAGCA-3′ and reverse: 5′-TGTAGTAGGCGATGCCACCT-3′;

sST2 (soluble isoform) forward: 5′-GCTCCAGGAACTCCAACCTC-3′ and reverse: 5′-AGCTCCAGGTACATCGGTGT-3′; GAPDH forward: 5′-CAGCCTCAAGATCATCAGCA-3′ and GAPDH reverse: 5′-TGTGGTCATGAGTCCTTCCA-3′.

2.5 Co-culture System

Human umbilical vein endothelial cells (HUVECs) were obtained from the ATCC (Rockville, MD, USA), while the Human aortic vascular smooth muscle cells (HAVSMCs) were purchased from the Institute of Biochemistry and Cell Biology (Shanghai, China). Both HUVECs and HAVSMCs were cultured in RPMI-1640 medium supplemented with 10% heat-inactivated FBS (HyClone, Logan, UT, USA), 1% penicillin and 1% streptomycin. To establish an indirect co-culture system, a Transwell chamber comprising a culture insert with a 10-µm thick porous membrane featuring 0.4-µm pores was used. In this system, foam cells (1×10^5 cells/well) from various transfection groups or ox-LDL preprocessed groups were initially seeded in the upper layer of the Transwell, placed within the wells of a six-well plate, and co-cultured with either HUVECs or HAVSMCs positioned at the bottom of the Transwell chamber (Corning, NY, USA). For co-culture experiments, HUVECs were seeded at a density of 1×10^5 cells per well and HAVSMCs at 5×10^4 cells per well in the lower compartment. All cell lines were validated by STR profiling and tested negative for mycoplasma.

2.6 Flow Cytometry Assay

Apoptosis was quantified by flow cytometry using an Annexin V-FITC/PI Apoptosis Detection Kit (Cat# KGA108, KeyGen Biotech, Nanjing, Jiangsu, China) according to the manufacturer's protocol. Briefly, cells were harvested with trypsin-EDTA, washed twice with PBS, and stained with FITC-labeled Annexin V (1 µg/mL) and propidium iodide (PI, 10 µg/mL) for 20 min in the dark. Samples were then analyzed on a FACScan flow cytometer (Beckman Coulter, Brea, CA, USA).

2.7 Immunofluorescence

The expression of ASS1 and NLRP3 in foam cells, and of the endothelial marker CD34 in HUVECs, was examined by immunofluorescence. Cells were seeded in sterile Millicell® EZ-Slide eight-well glass plates (PEZGS0816; Millipore, MA, USA). After reaching appropriate confluency, they were rinsed with PBS, fixed with 4% paraformaldehyde for 15 min, and permeabilized with 0.1% Triton X-100 for 30 min. Non-specific binding was blocked with 3% bovine serum albumin (BSA) for 1 h at room temperature. Cells were then incubated overnight at 4 °C with primary antibodies diluted as follows: anti-ASS1 (ab172730, 1:100; Abcam, Cambridge, UK) and anti-NLRP3 (ab270449,

1:100; Abcam) for foam cells, or anti-CD34 (ab81289, 1:200; Abcam) for HUVECs. After washing, samples were incubated for 2 h with a FITC-conjugated secondary antibody (BA1105, Boster, Wuhan, Hubei, China). Nuclei were counterstained with DAPI (10 µg/mL) for 5 min in the dark. Following final PBS washes, fluorescence images were acquired using a fluorescence microscope (Leica, Wetzlar, Germany).

2.8 Cell Counting Kit-8 (CCK-8) Assay

Cell viability of HAVSMCs was assessed using the Cell Counting Kit-8 (HY-K0301, CCK-8; MedChem Express, Monmouth Junction, NJ, USA). Cells from different experimental groups were seeded in 96-well plates. After the respective treatments, 10 µL of CCK-8 solution was added to each well, followed by incubation at 37 °C for 2 h. Absorbance was then measured at 450 nm using a microplate reader.

2.9 EdU Incorporation Assay

Cell proliferation was evaluated using the Cell-Light EdU Apollo®567 *In Vitro* Imaging Kit (C10371-1, RiboBio, Guangzhou, Guangdong, China) according to the manufacturer's instructions. HAVSMCs in logarithmic growth phase were seeded into 96-well plates at a density of 4×10^3 cells per well and cultured for 24 h. Cells were then pulsed with 50 µM EdU for 2 h, followed by fixation with 4% paraformaldehyde in PBS for 30 min. After washing with PBS, samples were incubated with 1× Apollo staining solution for 30 min, then permeabilized with 0.5% Triton X-100 in PBS for 10 min. Nuclei were counterstained with 1× Hoechst 33342 for 30 min at room temperature. Following a final PBS wash, EdU-positive cells were visualized and quantified under a fluorescence microscope.

2.10 Transwell Assay

Cell migration and invasion assays were performed using Transwell® chambers (Corning Life Sciences, Corning, NY, USA). For migration, uncoated inserts were used; for invasion, inserts pre-coated with Matrigel® matrix were employed. HAVSMCs were suspended in 100 µL of serum-free RPMI-1640 medium and seeded into the upper chamber. The lower compartment was filled with 500 µL of complete medium containing 10% FBS to serve as a chemoattractant. After incubation for 24 h at 37 °C under 5% CO_2, cells that had migrated or invaded to the lower surface of the membrane were fixed with methanol, stained with 0.1% crystal violet for 35 min, and counted in five randomly selected fields per insert under a light microscope.

2.11 Western Blot Analysis

Total cellular protein was extracted using RIPA lysis buffer (Pierce, Thermo Fisher Scientific), and protein concentration was determined by Bradford assay (Bio-Rad, Hercules, CA, USA). Protein samples (30 µg per lane) were separated on 12% SDS-PAGE gels and transferred onto PVDF membranes. After blocking with 5% non-fat milk for 1 h at room temperature, membranes were incubated overnight at 4 °C with the following primary antibodies (all from Abcam, unless otherwise noted): anti-ASS1 (ab172730), anti-ICAM-1 (ab282575), anti-VCAM-1 (ab134047), anti-STAT3 (ab68153), anti-phospho-STAT3 (ab267373), anti-ST2 (total; ab194113), anti-sST2 (soluble isoform; ab272372), anti-SMHC (ab133567), anti-CNN1 (ab46794), anti-α-SMA (ab7817), and anti-β-actin (ab8226). All Abcam antibodies were used at 1:1000 dilution, except β-actin (1:5000). To assess mitochondrial apoptosis in ASS1-treated HUVECs, additional blots were probed with anti-cleaved PARP (ab32561), anti-Bax (ab32503), and anti-Bcl-2 (ab32124). Following primary antibody incubation, membranes were washed and probed with a horseradish peroxidase-conjugated secondary antibody (sc-2004, Santa Cruz Biotechnology, Dallas, TX, USA) for 1 h at room temperature. Protein bands were visualized using enhanced chemiluminescence (ECL) substrate (Thermo Fisher Scientific) and imaged with a chemiluminescence detection system.

2.12 Enzyme-Linked Immunosorbent Assay (ELISA)

IL-33 levels in foam cell supernatants and IL-1β levels in mouse serum were quantified using commercially available ELISA kits (IL-33 ELISA Kit (Cat# SEA568Hu), IL-1β ELISA Kit (Cat# SEA563Mu), Cloud-Clone Corp, Wuhan, Hubei, China) according to the manufacturer's protocols. Briefly, samples and standards (100 µL each) were added to the wells of a 96-well plate and incubated at 37 °C for 90 min. After washing three times, 100 µL of biotinylated detection antibody was added and incubated for 60 min. Following another wash step, 100 µL of horseradish peroxidase (HRP)-conjugated streptavidin working solution was applied for 30 min. Color development was initiated by adding substrate solution, and the reaction was stopped before absorbance was measured at 450 nm and 630 nm using a microplate reader (Thermo Fisher Scientific).

2.13 TUNEL Staining

Apoptotic endothelial cells were detected by TUNEL staining using a fluorescence FITC kit (12156792910, Roche, Indianapolis, IN, USA) according to the manufacturer's instructions. HUVECs grown on coverslips were fixed with 4% paraformaldehyde and permeabilized with 0.1% Triton X-100. After washing, cells were incubated with the TUNEL reaction mixture for 1 h at 37 °C in the dark. Following three washes with PBS, nuclei were counterstained with DAPI (10 µg/mL; Solarbio, Beijing, China). Images were captured using a fluorescence microscope (Olympus BX51, Tokyo, Japan) at 200× magnification. TUNEL-positive cells, identified by green nuclear fluorescence, were quantified in at least five random fields per sample.

2.14 Construction of Atherosclerosis Mouse Model

Male apolipoprotein E-deficient ($ApoE^{-/-}$) mice were obtained from the Laboratory Animal Center of Fuwai Hospital, National Center for Cardiovascular Diseases. All animal procedures were approved by the Institutional Animal Care and Use Committee of Peking Union Medical College (Approval No. 0105-1-6-ZX(X)-4). Mice were housed under specific pathogen-free conditions with a 12 h light/dark cycle and free access to food and water. Atherosclerosis was induced by feeding 8-week-old mice a high-fat diet (21% fat, 0.15% cholesterol, 3.2% cholate) for 12 weeks. Body weight and food intake were recorded weekly.

After the 12-week dietary intervention (high-fat diet #D12079B, Research Diets Inc., New Brunswick, NJ, USA), mice were euthanized in strict accordance with institutional animal care guidelines. Euthanasia was performed via intraperitoneal injection of sodium pentobarbital (Euthasol®) at a dose of 200 mg kg^{-1} body weight. The stock solution (39% w/v) was diluted 1:10 with 0.9% saline to obtain a 3.9% w/v working solution. Prior to injection, mice were gently restrained to minimize stress. Depth of anesthesia was confirmed by loss of pedal reflex and cessation of spontaneous respiration. Following this confirmation, euthanasia was carried out as a result of the administered pentobarbital overdose, leading to cardiac arrest. Cardiac arrest was verified by thoracotomy within 5 min of respiratory cessation. Cervical dislocation was performed immediately after cardiac arrest as a secondary physical method to ensure death. All procedures were conducted by trained personnel between 08:00 and 11:00 to minimize circadian influences. Tissues were subsequently harvested for analysis.

2.15 AAV9-Mediated ASS1 Knockdown and Overexpression

To modulate mouse ASS1 (NCBI reference: NM_007494.3) expression *in vivo*, adeno-associated virus serotype 9 (AAV9) vectors were constructed for overexpression and knockdown. For overexpression, the full-length ASS1 coding sequence was subcloned into the pcDNA3.1 plasmid (Invitrogen, Carlsbad, CA, USA) and then inserted into the AAV9 backbone plasmid pAV-F4/80 (Weizhen Biotechnology Co., Jinan, Shandong, China). For knockdown, potential shRNA target sites were screened by co-transfecting the pcDNA3.1-ASS1 plasmid and the pAV-CAG-GFP-mir30 shRNA library plasmid (Boshang Biotechnology Co., Jinan, Shandong, China) into HEK-293 cells. The most efficient shRNA sequence was subsequently cloned into the pAV-F4/80-GFP-mir30 shRNA vector (Wuyue Biotechnology Co., Jinan, Shandong, China) and packaged into AAV9 particles. Control vectors included AAV9 expressing a scrambled shRNA (for knockdown experiments) and empty pAV-F4/80 (for overexpression experiments).

Mice were randomly assigned to five groups: (1) wild-type sham, (2) atherosclerosis model, (3) negative control (empty vector), (4) ASS1 knockdown, and (5) ASS1 overexpression. After 12 weeks of a high-fat diet, mice received an intravenous injection of the respective AAV9 vector (1×10^{12} vp/mL, 50 µL per mouse) via the tail vein without anesthesia to minimize stress and physiological disturbance. Four weeks post-injection, all mice were euthanized for tissue collection. Prior to euthanasia, mice were deeply anesthetized with an intraperitoneal injection of sodium pentobarbital (200 mg/kg). Adequate depth of anesthesia was confirmed by the loss of the pedal reflex. Following anesthesia, tissues were harvested for subsequent analyses. All animal procedures were performed in accordance with institutional animal care guidelines.

2.16 Histological Analysis of Atherosclerotic Plaques

Plaque lipid content was evaluated by Oil Red O staining. Tissue samples from the transverse cardiac section (TCS) and aortic arch (AAC) were fixed in 10% neutral-buffered formalin for 24 h at room temperature, embedded in paraffin, and sectioned at 5 µm. Sections were deparaffinized in xylene, rehydrated through a graded ethanol series (100% → 95% → 80% → 70%), and rinsed in distilled water.

Sections were stained with Oil Red O working solution (prepared by dissolving Oil Red O powder [Sigma-Aldrich, Cat. No. O0625] in isopropanol and diluting with distilled water at a 3:2 ratio) for 15 min at room temperature. After rinsing with distilled water, nuclei were counterstained with hematoxylin (Merck, Cat. No. 109297) for 1 min, differentiated in 70% ethanol, and mounted with neutral mounting medium. Lipid droplets were visualized as red areas under a light microscope.

The Oil Red O-positive area was quantified as a percentage of total plaque area using image-analysis software. For each mouse, three non-consecutive sections were analyzed, and the mean value was used for statistical comparisons (n = 6 mice per group).

2.17 Statistical Analysis

Data are presented as mean ± standard error of the mean (SD). Comparisons between two groups were performed using Student's *t*-test. For multiple-group comparisons, one-way analysis of variance (ANOVA) with repeated measures was applied, followed by Tukey's post-hoc test for pairwise comparisons. A p-value < 0.05 was considered statistically significant. All statistical analyses were conducted using GraphPad Prism version 8.0 (GraphPad Software, San Diego, CA, USA).

3. Results

3.1 ASS1 Expression is Elevated in Foam Cells In Vitro

To examine the role of ASS1 in atherosclerosis, foam cells were generated by treating U937 human monocytes

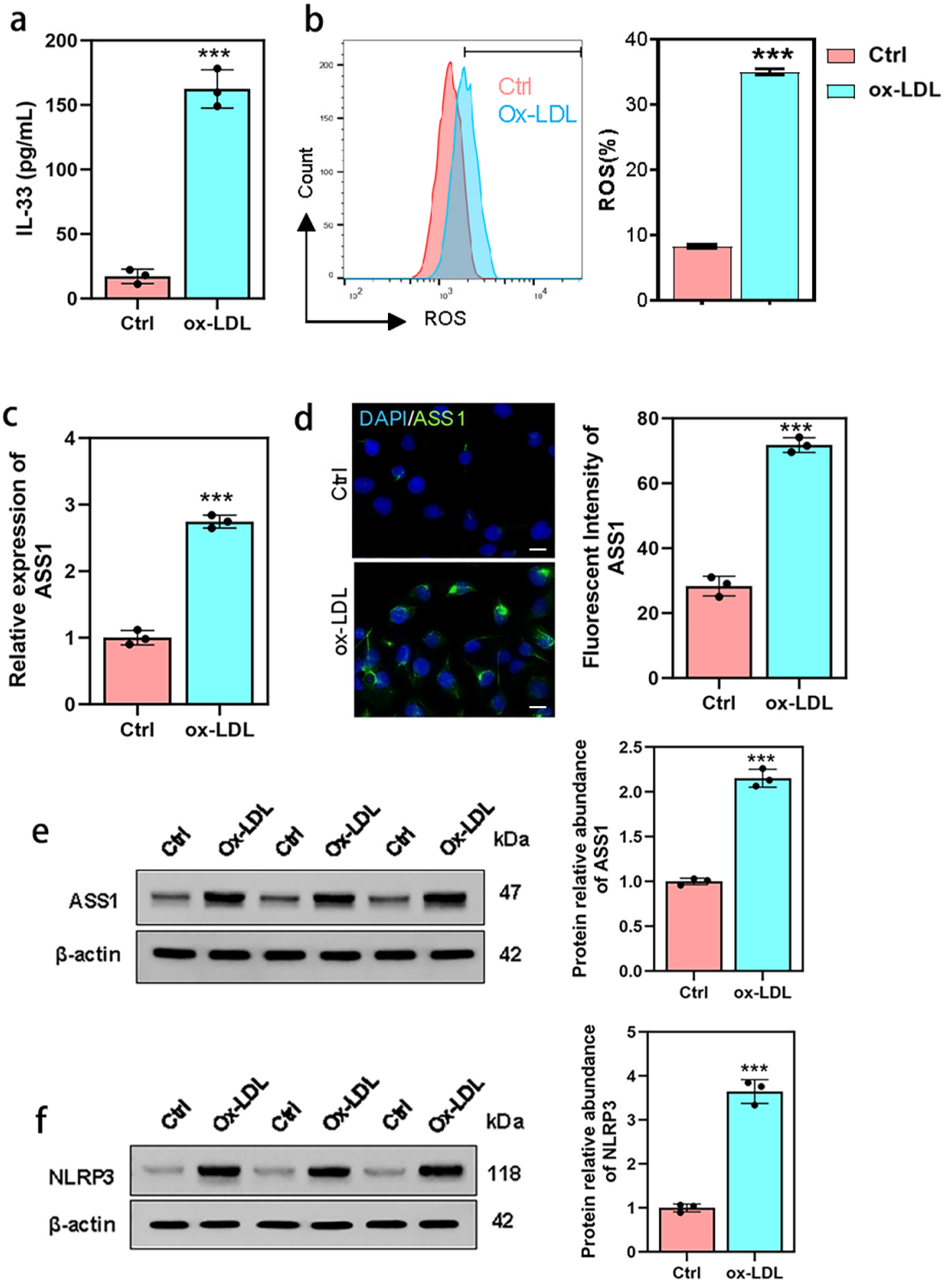

Fig. 1. ASS1 expression is upregulated in ox-LDL-induced U937 foam cells. U937 foam cells were generated through co-treatment with 100 nM phorbol 12-myristate 13-acetate (PMA) for 48 h and 50 µg/mL oxidized low-density lipoprotein (ox-LDL) for an additional 48 h. (a) IL-33 concentration measured by ELISA assay. (b) ROS generation analyzed by flow cytometry. (c) ASS1 expression assessed via quantitative real-time PCR. (d) Immunofluorescence assay and (e) Western blot showing ASS1 expression in foam cells. (f) Western blot analysis demonstrating NLRP3 expression in foam cells. The scale bar is 50 µm in (d). For all panels, n = 3 biologically independent experiments, each performed on separate days with 1×10^6 cells per well; technical replicates: 3 wells per condition per biological replicate. Data are presented as mean ± standard deviation (SD), error bars indicate SD. Statistical significance was evaluated by one-way analysis of variance (ANOVA) followed by Tukey's post-hoc test. ***$p < 0.001$ versus the control group.

with phorbol 12-myristate 13-acetate (PMA) and oxidized low-density lipoprotein (ox-LDL). ELISA showed that PMA + ox-LDL treatment significantly increased IL-33 secretion (Fig. 1a), and flow cytometry confirmed elevated intracellular reactive oxygen species (ROS) levels (Fig. 1b), confirming successful foam cell differentiation.

ASS1 expression was then evaluated in these cells. qPCR analysis revealed a marked upregulation of ASS1 mRNA in foam cells compared with untreated controls (Fig. 1c). Consistent with this, both immunofluorescence and Western blotting demonstrated increased ASS1 protein expression in foam cells (Fig. 1d,e). Interestingly, Western blot also indicated an upward trend in NLRP3 protein levels in foam cells (Fig. 1f).

3.2 ASS1 Promotes ROS Production and Inflammatory Activation in Ox-LDL-Induced Foam Cells

To determine the functional role of ASS1 in foam cells, we modulated its expression by siRNA-mediated knockdown and plasmid-mediated overexpression. qPCR confirmed efficient reduction of ASS1 mRNA after si-ASS1 transfection and increased expression after ASS1 overexpression (Fig. 2a).

Intracellular ROS levels, measured by DCFH-DA fluorescence, were elevated in ox-LDL-treated foam cells. ASS1 knockdown significantly attenuated this increase, whereas ASS1 overexpression further enhanced ROS production (Fig. 2b,c).

Western blotting verified the corresponding changes in ASS1 protein (Fig. 2d,e). Notably, ASS1 knockdown reduced the protein levels of the adhesion molecules ICAM-1 and VCAM-1, while ASS1 overexpression increased them (Fig. 2e). Phosphorylation of STAT3 (p-STAT3) was also diminished by ASS1 knockdown and augmented by ASS1 overexpression (Fig. 2f).

Consistent with these pro-inflammatory changes, IL-33 secretion—quantified by ELISA—was decreased upon ASS1 knockdown and elevated upon ASS1 overexpression (Fig. 2g). Together, these data indicate that ASS1 drives oxidative stress and inflammatory activation in ox-LDL-stimulated foam cells.

3.3 STAT3 is Required for ASS1-Mediated NLRP3 Activation and IL-33 Secretion in Foam Cells

To determine whether ASS1 acts through STAT3 signaling, rescue experiments were conducted using STAT3-specific siRNA (si-STAT3) and a constitutively active STAT3 mutant (STAT3-CA) in U937 foam cells. Western blot analysis revealed that ASS1 overexpression upregulated NLRP3, ICAM-1, and VCAM-1, an effect that was largely abolished by co-transfection with si-STAT3 (Fig. 3a). Conversely, expression of STAT3-CA reversed the downregulation of these proteins caused by ASS1 knockdown (Fig. 3a).

ASS1 overexpression increased STAT3 phosphorylation (p-STAT3), while ASS1 knockdown reduced it; these changes were respectively blocked by si-STAT3 or restored by STAT3-CA (Fig. 3b). Similarly, ASS1-induced elevation of ROS production and IL-33 secretion was suppressed by si-STAT3, whereas the decreases resulting from ASS1 knockdown were rescued by STAT3-CA (Fig. 3c–e).

Collectively, these data demonstrate that STAT3 activation is an essential downstream event through which ASS1 promotes NLRP3 inflammasome activity and IL-33 release in foam cells.

3.4 ASS1 Promotes HUVEC Apoptosis in Co-Culture With Foam Cells

To further examine the role of ASS1 in ox-LDL-induced endothelial injury, we co-cultured HUVECs with U937-derived foam cells. Apoptosis was significantly increased in HUVECs exposed to ox-LDL-induced foam cells, as shown by flow cytometry (Fig. 4a). This effect was attenuated by ASS1 knockdown in foam cells and further exacerbated by ASS1 overexpression, which was confirmed by TUNEL staining (Fig. 4b).

Western blot analysis of HUVECs revealed that ASS1 knockdown reduced the levels of cleaved PARP and Bax while increasing Bcl-2, whereas ASS1 overexpression had the opposite effect. The Bax/Bcl-2 ratio was approximately 3-fold higher in the ASS1-overexpression group than in the vector control, indicating activation of the mitochondrial apoptosis pathway (**Supplementary Fig. 1**).

Immunofluorescence staining showed that the endothelial marker CD34 was not altered by ASS1 manipulation in foam cells (Fig. 4c). Interestingly, while co-culture with ox-LDL-induced U937 foam cells significantly enhanced total ST2 expression in HUVECs, these levels were maintained independently of ASS1 manipulation (knockdown or overexpression) (Fig. 4d).

These data suggest that ASS1 in foam cells enhances ox-LDL-driven endothelial apoptosis through the mitochondrial pathway, without affecting endothelial marker expression or total ST2 levels.

3.5 ASS1 Shifts the ST2 Isoform Balance Toward a Pro-Inflammatory Profile in Foam Cells and Co-Cultured Vascular Cells

Given the opposing roles of the soluble decoy receptor sST2 and the membrane-bound signaling receptor ST2L, we examined how ASS1 regulates their expression. In U937 foam cells, ASS1 overexpression significantly increased sST2 mRNA and decreased ST2L mRNA, raising the sST2/ST2L ratio. Conversely, ASS1 knockdown reduced sST2 and increased ST2L mRNA, lowering the sST2/ST2L ratio (**Supplementary Fig. 2a,b**).

A similar regulatory pattern was observed in HUVECs and HAVSMCs co-cultured with ASS1-modulated foam cells. Co-culture with ASS1-overexpressing

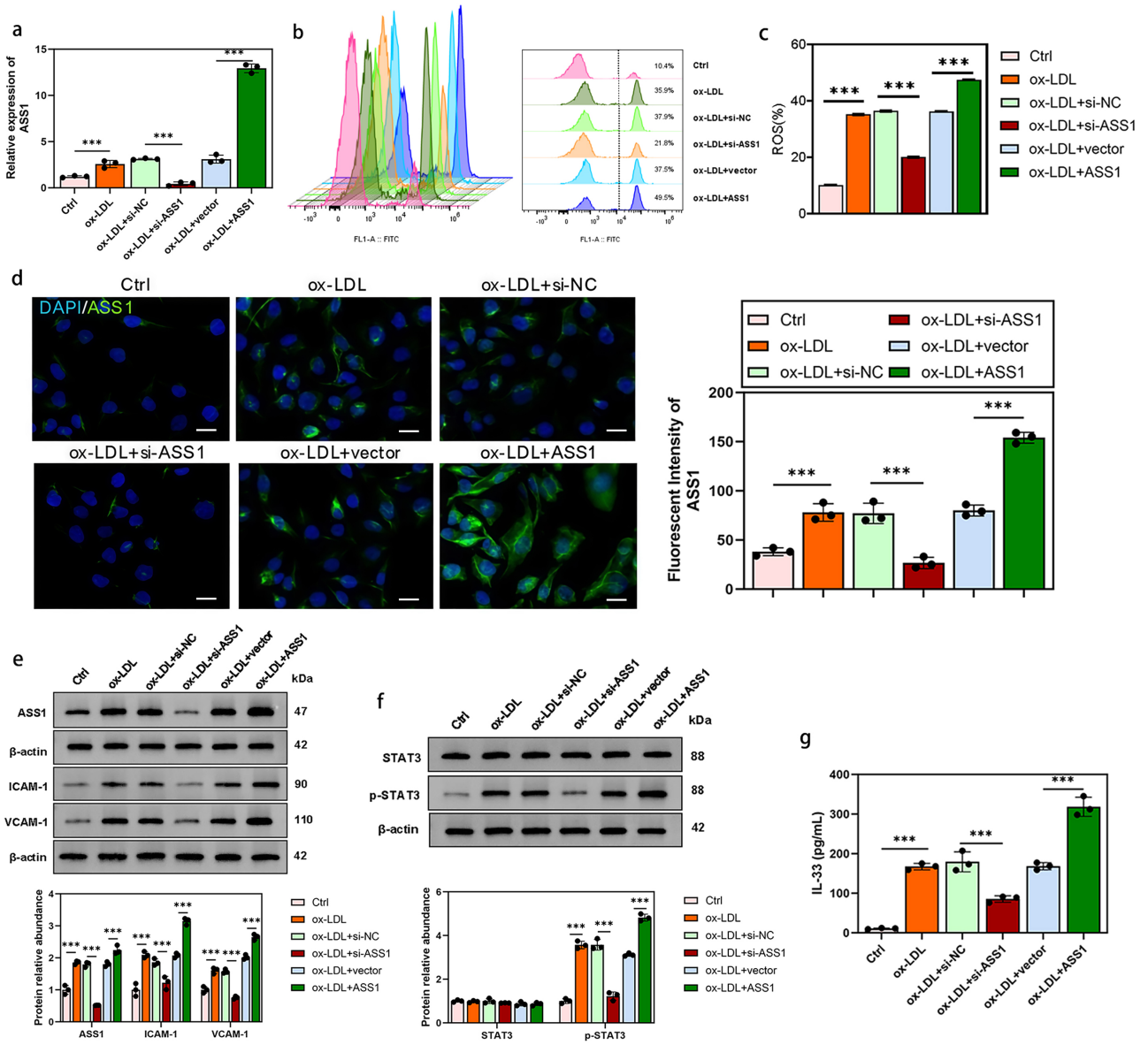

Fig. 2. ASS1 modulates ROS production, inflammatory marker expression, and IL-33 secretion in foam cells. U937 foam cells were transfected with si-ASS1 or ASS1 overexpression plasmid for 48 h. (a) Quantitative real-time PCR analysis of ASS1 mRNA expression. (b,c) Flow cytometry analysis of ROS generation. (d) Immunofluorescence assay showing ASS1 protein levels. (e) Western blot analysis of ASS1, ICAM-1, VCAM-1, (f) STAT3, and p-STAT3 protein levels. (g) ELISA assay for IL-33 concentration. The scale bar is 50 μm in (d). For all panels, n = 3 biologically independent experiments (performed on different days with different cell passages, 1×10^6 cells per well); technical replicates: 3 wells per condition in each biological replicate. Data are presented as mean ± standard deviation (SD), and error bars indicate SD. Statistical significance: ***$p < 0.001$ versus the corresponding baseline by one-way ANOVA with Tukey's post-hoc test.

foam cells elevated sST2 mRNA and reduced ST2L mRNA in both HUVECs (**Supplementary Fig. 2c,d**) and HAVSMCs (**Supplementary Fig. 2e,f**), again increasing the sST2/ST2L ratio. Western blot analysis confirmed these changes at the protein level: ASS1 overexpression in foam cells increased sST2 protein in co-cultured HUVECs (**Supplementary Fig. 2g**) and HAVSMCs (**Supplementary Fig. 2h**), whereas ASS1 knockdown produced the opposite effect.

Together, these findings indicate that ASS1 drives a shift in the ST2 isoform balance toward a pro-inflammatory state—characterized by elevated sST2 and reduced ST2L—thereby potentiating IL-33-mediated signaling activity.

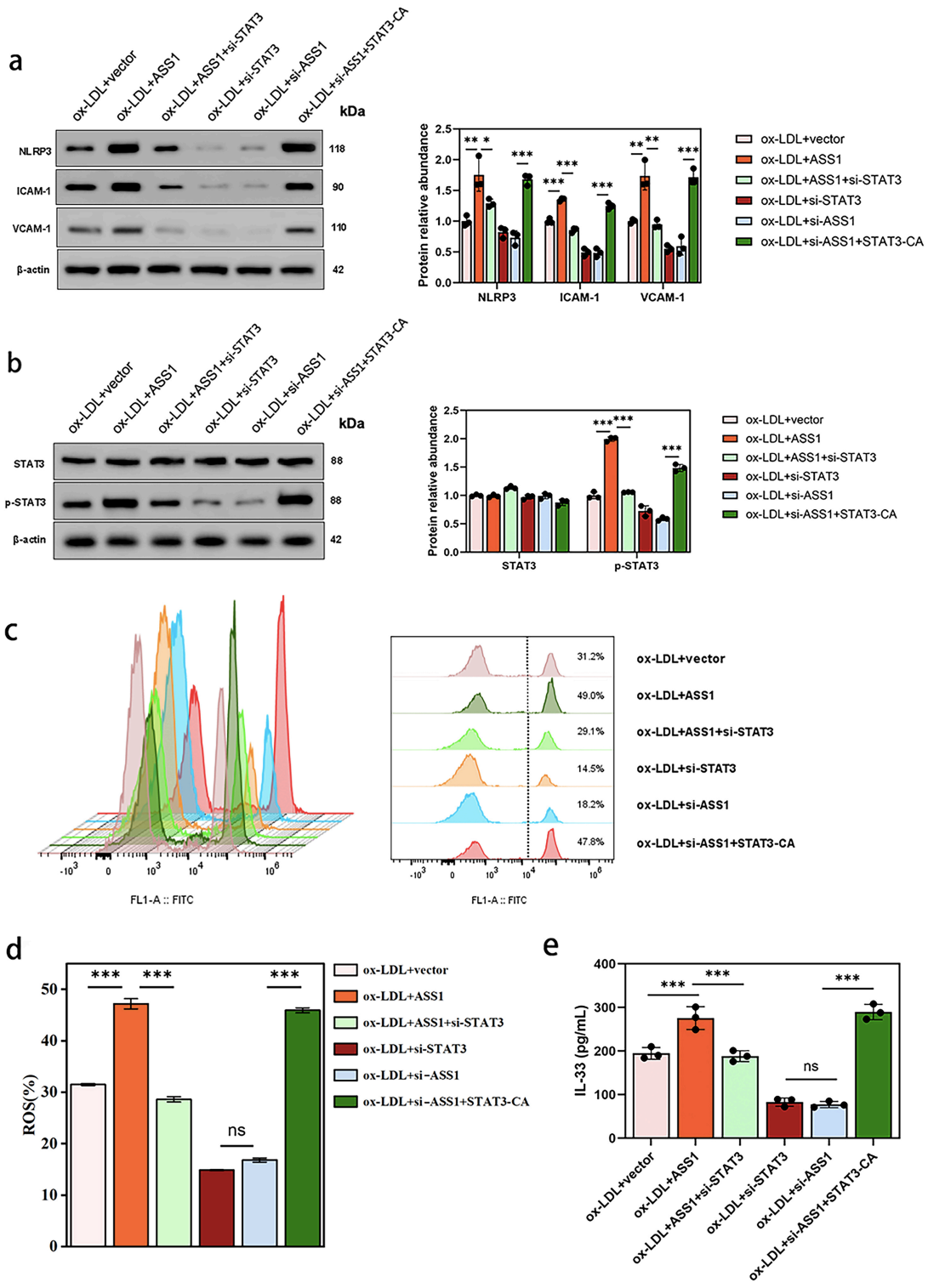

Fig. 3. ASS1 regulates NLRP3 inflammasome activation and IL-33 secretion through STAT3 phosphorylation in U937 foam cells. Foam cells were co-transfected with indicated plasmids/siRNAs and treated with ox-LDL (50 μg/mL). The experimental groups were as follows: ox-LDL + vector, ox-LDL + ASS1, ox-LDL + ASS1 + si-STAT3, ox-LDL + si-STAT3, ox-LDL + si-ASS1, and ox-LDL + si-ASS1 + STAT3-CA. (a) Western blot analysis of NLRP3, ICAM-1, and VCAM-1 expression. (b) STAT3 and p-STAT3 protein levels. (c,d) ROS production measured by DCFH-DA flow cytometry. (e) IL-33 concentration determined by ELISA. For all panels, n = 3 biologically independent experiments (performed on different days, 1×10^6 cells per well); technical replicates: 3 wells per condition in each biological replicate. Data are presented as mean ± standard deviation (SD). Error bars represent SD. ns, not significant ($p \geq 0.05$), *$p < 0.05$, **$p < 0.01$, ***$p < 0.001$ by one-way ANOVA with Tukey post-hoc test relative to the corresponding baseline.

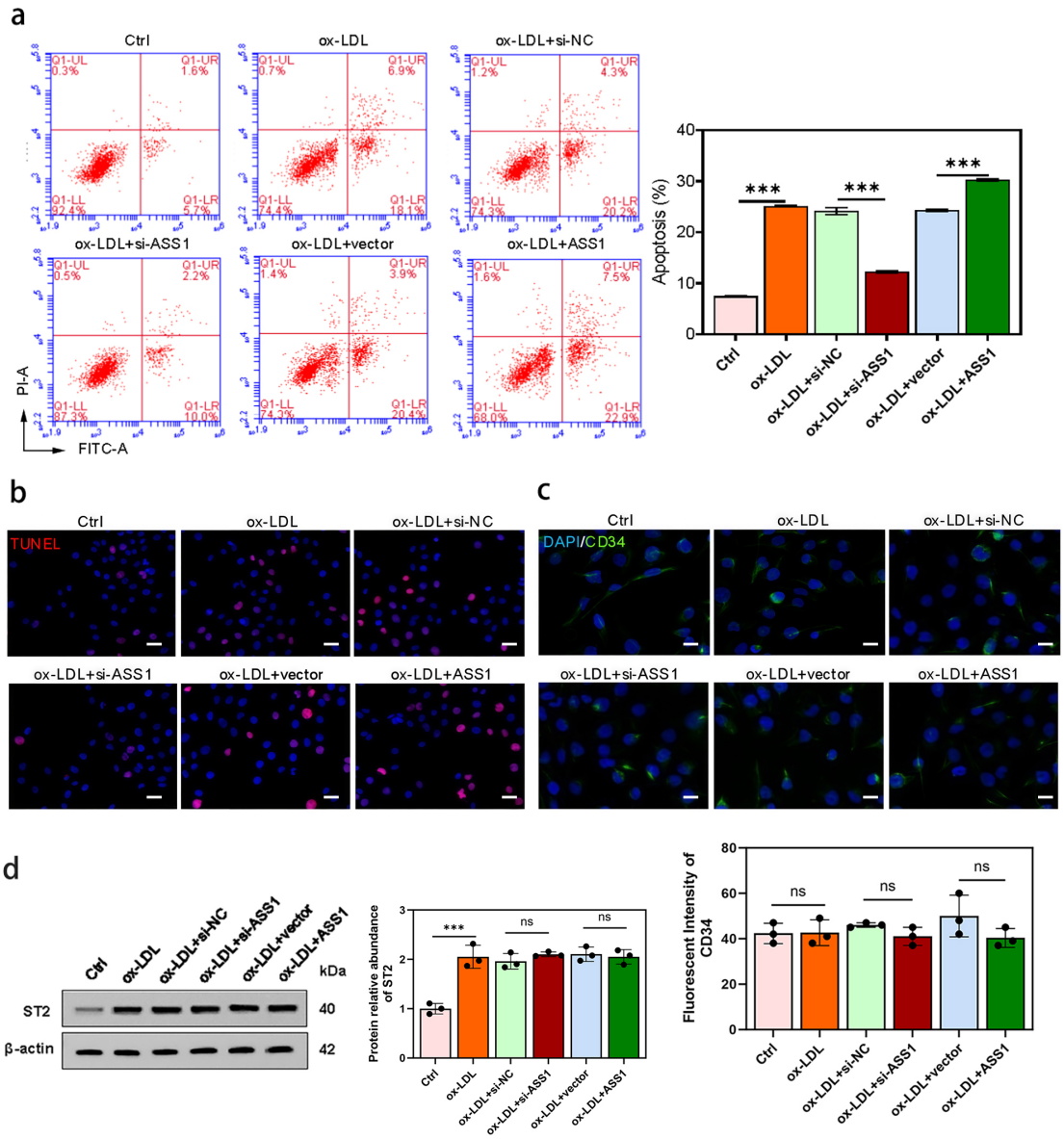

Fig. 4. ASS1 in foam cells promotes HUVEC apoptosis via the mitochondrial pathway without affecting CD34 or total ST2 expression. HUVECs were co-cultured with U937 foam cells from control, si-NC, si-ASS1, vector, and ASS1 groups. (a) Flow cytometry analysis of the apoptotic rate of endothelial cells. (b) TUNEL fluorescence FITC assay for apoptotic endothelial cells. (c) Immunofluorescence staining of the vascular marker CD34. (d) Western blot analysis of ST2 protein levels. The scale bar is 50 µm in (b,c). For all panels, n = 3 biologically independent experiments (performed on different days with different HUVEC donors and different U937 passages); each experiment used 1×10^5 HUVECs per well (12-well plate) and 2×10^5 U937 foam cells per insert, with 3 technical replicates per group. Data are presented as mean ± standard deviation (SD). Error bars represent SD. ***$p < 0.001$, ns, no significance (one-way ANOVA with repeated measures and Tukey post-hoc test relative to corresponding baseline).

3.6 ASS1 Promotes Proliferation, Migration, and Dedifferentiation of HAVSMCs Co-Cultured With Foam Cells

Given the contribution of vascular smooth muscle cells (VSMCs) to atherosclerotic plaque progression, we examined whether ASS1 in foam cells influences HAVSMC behavior. HAVSMCs were co-cultured with ox-LDL-induced U937 foam cells in which ASS1 was either knocked down or overexpressed.

CCK-8 and EdU assays showed that ox-LDL-treated foam cells stimulated HAVSMC proliferation, an effect that was further enhanced by ASS1 overexpression and reduced by ASS1 knockdown (Fig. 5a,b).

Western blot analysis revealed that co-culture with ox-LDL-induced foam cells downregulated the VSMC differentiation markers SMHC, CNN1, and α-SMA in HAVSMCs. This downregulation was partially reversed by ASS1 knockdown in foam cells and exacerbated by ASS1

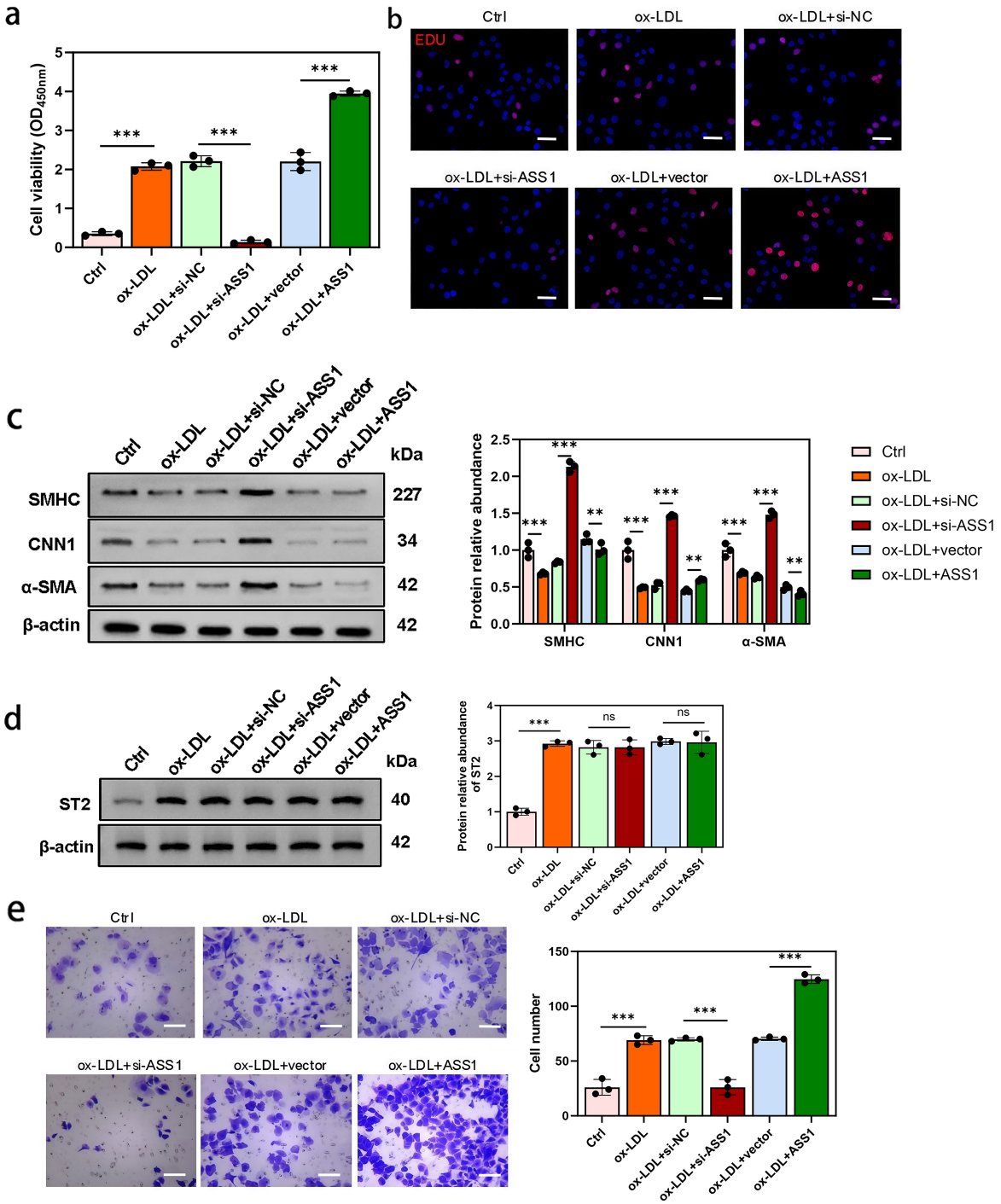

Fig. 5. ASS1 in foam cells promotes HAVSMC proliferation, migration, and dedifferentiation. HAVSMCs were co-cultured with U937 foam cells from control, si-NC, si-ASS1, vector, and ASS1 groups. (a) Cell viability was assessed by the CCK-8 assay. (b) Cell proliferation of HAVSMCs was evaluated using EdU staining. (c) Western blot analysis of SMHC, CNN1, and α-SMA protein levels. (d) Western blot analysis of ST2 protein levels. (e) Transwell assay to determine cell migration and invasion in HAVSMCs. The scale bar is 50 μm in (b), and the scale bar is 100 μm in (e). For all panels, n = 3 biologically independent experiments (performed on different days with different HAVSMC lots and different U937 passages); each experiment used 1×10^4 HAVSMCs per well (96-well plate for CCK-8, 24-well plate for EdU, 6-well plate for Western blot, and 24-well Transwell inserts for migration/invasion) with 3 technical replicates per group. Data presented as mean ± standard deviation (SD). Error bars represent SD. ns, not significant ($p \geq 0.05$), $^{**}p < 0.01$, $^{***}p < 0.001$ by one-way ANOVA with Tukey post-hoc test relative to the corresponding baseline.

overexpression (Fig. 5c), indicating that ASS1 promotes VSMC dedifferentiation.

Notably, total ST2 protein levels in HAVSMCs were elevated following co-culture with ox-LDL-treated foam cells, but were not significantly altered by modulating ASS1 expression in foam cells (Fig. 5d).

Finally, Transwell migration assays demonstrated that ASS1 knockdown in foam cells attenuated the enhanced migration of HAVSMCs induced by co-culture, whereas ASS1 overexpression further increased migratory capacity (Fig. 5e).

Together, these results indicate that ASS1 in foam cells drives HAVSMC proliferation, migration, and dedifferentiation—key processes in atheroma progression—without affecting total ST2 expression in co-cultured HAVSMCs.

3.7 NLRP3 Overexpression Rescues ASS1-Mediated Inflammatory Activation and ROS Production in Foam Cells

To determine whether NLRP3 mediates the pro-inflammatory effects of ASS1, rescue experiments were performed in U937 foam cells. ELISA showed that ASS1 knockdown reduced IL-33 secretion, and this reduction was largely reversed by NLRP3 overexpression (Fig. 6a). Similarly, the decrease in ROS production caused by ASS1 knockdown was restored upon NLRP3 overexpression (Fig. 6b,c).

Immunofluorescence confirmed successful NLRP3 overexpression (Fig. 6d). ASS1 protein downregulation by siRNA was not altered by NLRP3 overexpression (Fig. 6e), indicating that NLRP3 acts downstream of ASS1.

Western blot analysis revealed that the downregulation of adhesion molecules (ICAM-1 and VCAM-1) induced by ASS1 knockdown was abolished by NLRP3 overexpression (Fig. 6f). Likewise, the reduced expression of NLRP3 itself and its adaptor protein PYCARD after ASS1 knockdown was restored by NLRP3 overexpression (Fig. 6g). In contrast, NLRP3 overexpression did not reverse the decrease in STAT3 phosphorylation (p-STAT3) caused by ASS1 knockdown (Fig. 6h).

These results demonstrate that NLRP3 activation is a key downstream event responsible for ASS1-driven inflammatory signaling and oxidative stress in foam cells, independent of changes in ASS1 expression or STAT3 phosphorylation.

3.8 NLRP3 Overexpression Alone Recapitulates the Pro-Inflammatory Effects of ASS1 in Foam Cells

To determine whether NLRP3 activation itself is sufficient to induce ASS1-like inflammatory responses, we overexpressed NLRP3 alone in ox-LDL-treated U937 foam cells without altering ASS1 expression. Western blot analysis showed that NLRP3 overexpression significantly increased the protein levels of adhesion molecules ICAM-1 and VCAM-1 (Fig. 7a), as well as NLRP3 and its adaptor protein PYCARD (Fig. 7b), to a degree comparable to ASS1 overexpression.

Flow cytometry revealed that NLRP3 overexpression alone markedly elevated intracellular ROS production (Fig. 7c,d), similar to the effect of ASS1 overexpression. ELISA further demonstrated that IL-33 secretion was increased by approximately 70% in NLRP3-overexpressing cells, with no statistically significant difference from the ASS1-overexpression group (Fig. 7e).

Importantly, the anti-inflammatory effects of ASS1 knockdown—reduced ROS, lower adhesion molecule expression, and decreased IL-33 secretion—were largely reversed when NLRP3 was co-overexpressed (Fig. 7a–e).

Together, these results indicate that NLRP3 activation is sufficient to drive a pro-inflammatory phenotype in foam cells, and that the pro-atherogenic effects of ASS1 are mediated primarily through upregulation of NLRP3.

3.9 NLRP3 Overexpression Rescues ASS1-Mediated Effects on HUVECs and HAVSMCs in Co-Culture

We next examined whether NLRP3 modulates the impact of ASS1 on vascular cells using a foam-cell co-culture model.

HUVECs: ASS1 knockdown in foam cells reduced HUVEC apoptosis, an effect that was reversed by NLRP3 overexpression in foam cells, as shown by flow cytometry and TUNEL staining (Fig. 8a,b). The endothelial marker CD34 was unaffected by either ASS1 or NLRP3 manipulation (Fig. 8c). Total ST2 expression in HUVECs was elevated after co-culture with ox-LDL-induced foam cells, but remained elevated upon ASS1 knockdown or NLRP3 overexpression (Fig. 8d).

HAVSMCs: ASS1 knockdown in foam cells attenuated HAVSMC proliferation, which was restored by NLRP3 overexpression (CCK-8 and EdU assays; Fig. 9a,b). Western blotting showed that ASS1 knockdown increased the expression of smooth-muscle differentiation markers (SMHC, CNN1, α-SMA), an effect that was blunted by NLRP3 overexpression (Fig. 9c). Total ST2 levels in HAVSMCs were also raised after co-culture, independent of ASS1 or NLRP3 modulation (Fig. 9d). Furthermore, Transwell migration assays confirmed that the decreased HAVSMC migration caused by ASS1 knockdown was rescued by NLRP3 overexpression (Fig. 9e).

These results indicate that NLRP3 activation in foam cells can counteract the regulatory effects of ASS1 on endothelial apoptosis and smooth muscle proliferation/migration, whereas total ST2 expression in vascular cells is influenced by ox-LDL-exposed foam cells but not directly by ASS1 or NLRP3.

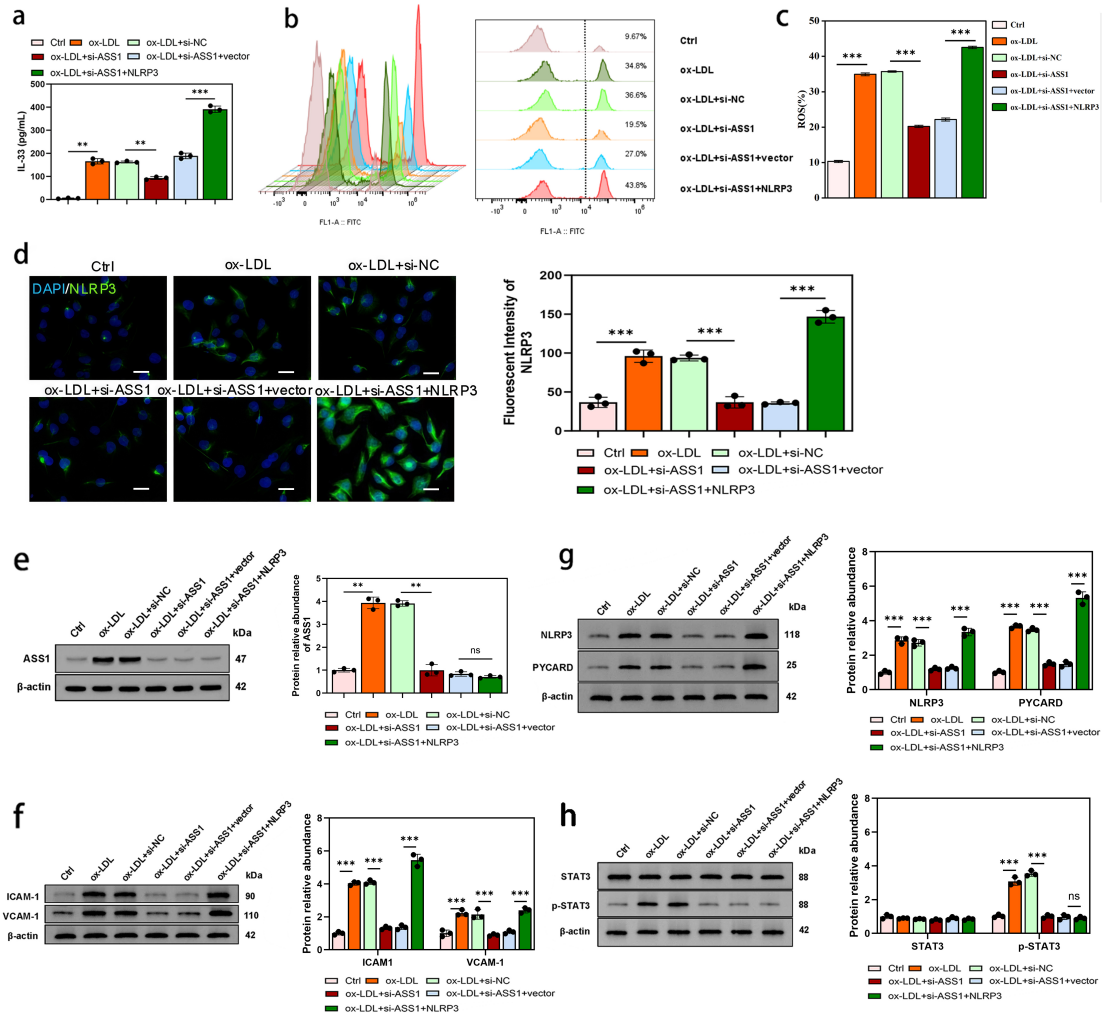

Fig. 6. NLRP3 overexpression rescues the anti-inflammatory effects of ASS1 knockdown in foam cells. U937 foam cells were co-transfected with si-ASS1 and NLRP3 overexpression plasmid or transfected with si-ASS1 alone. (a) IL-33 concentration determined by ELISA assay. (b,c) Flow cytometry analysis of ROS generation. (d) Immunofluorescence assay showing NLRP3 protein expression in U937 foam cells. (e) Western blot analysis of ASS1 protein levels. (f) Western blot analysis of adhesion molecules ICAM-1 and VCAM-1, (g) inflammasome-associated proteins NLRP3 and PYCARD, and (h) STAT3 and p-STAT3 associated with the STAT3 signaling pathway. The scale bar is 50 μm in (d). For all panels, n = 3 biologically independent experiments (performed on different days with different cell passages); each experiment contained 3 technical replicates (wells) per condition, with 2×10^5 U937 foam cells per well. Data are presented as mean ± standard deviation (SD). Error bars represent SD. ns, not significant ($p \geq 0.05$), $^{**}p < 0.01$, $^{***}p < 0.001$ by one-way ANOVA with Tukey post-hoc test relative to the corresponding baseline.

3.10 ASS1 Promotes Systemic Inflammation and Atherosclerotic Plaque Progression In Vivo

To further evaluate the role of ASS1 in atherosclerosis, we performed histological and biochemical analyses in ApoE-deficient mice. Mice were fed a high-fat diet for 12 weeks to induce atherosclerosis, after which ASS1 expression was modulated via AAV9 vectors. Plaques from the transverse cardiac section (TCS) and aortic arch (AAC) were examined.

Oil Red O staining showed that lipid accumulation was markedly increased in atherosclerotic (AS) mice compared with sham-operated controls (Fig. 10a). Quantification confirmed the most severe lipid deposition in the ASS1-overexpression ($ASS1^{OE}$) group, intermediate levels in the AS and negative control (NC) groups, and significantly reduced lipid in the ASS1-knockdown ($ASS1^{kd}$) group (Fig. 10b,c). Body weight was also highest in $ASS1^{OE}$ mice, while $ASS1^{kd}$ mice maintained weights similar to the Sham group, suggesting a systemic metabolic influence of ASS1 (Fig. 10d).

Western blot analysis of vascular tissues revealed that ASS1 overexpression increased NLRP3 protein levels, whereas ASS1 knockdown decreased them (Fig. 10e). Similarly, phosphorylated STAT3 (p-STAT3) was upregu-

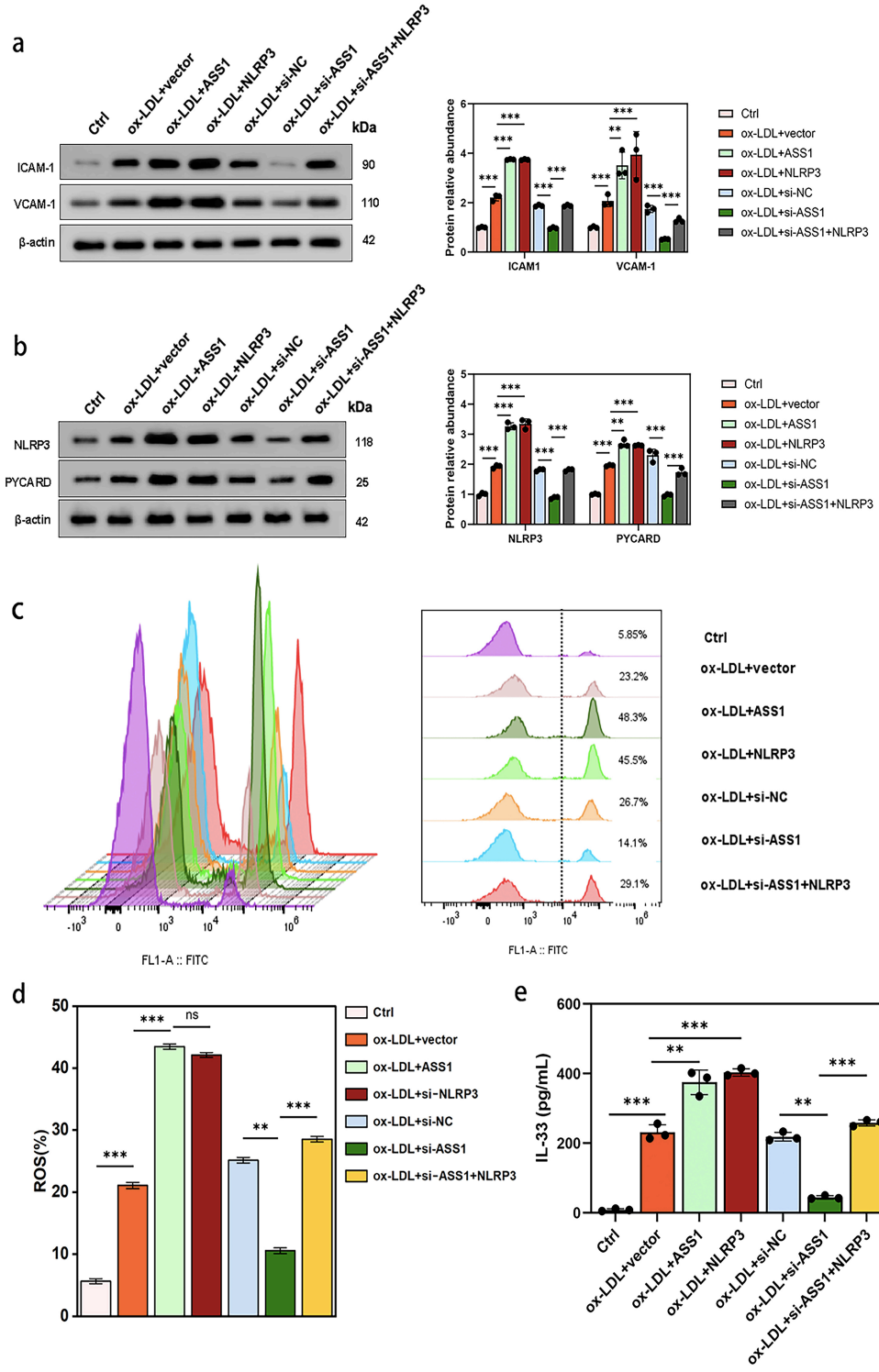

Fig. 7. NLRP3 overexpression increased downstream factors to levels comparable to ASS1 overexpression, and reversed the effects of ASS1 knockdown. U937 foam cells were treated as follows: Ctrl (untreated), ox-LDL + vector, ox-LDL + ASS1, ox-LDL + NLRP3, ox-LDL + si-NC, ox-LDL + si-ASS1, or ox-LDL + si-ASS1 + NLRP3. (a) Western blot analysis of adhesion molecules ICAM-1 and VCAM-1. (b) Inflammasome-associated proteins NLRP3 and PYCARD expression. (c,d) ROS production measured by DCFH-DA flow cytometry. (e) IL-33 concentration determined by ELISA assay. For all panels, n = 3 biologically independent experiments (performed on different days, 1×10^6 cells per well); technical replicates: 3 wells per condition in each biological replicate. Data are presented as mean ± standard deviation. ns, not significant ($p \geq 0.05$), $^{**}p < 0.01$, $^{***}p < 0.001$ by one-way ANOVA with Tukey post-hoc test relative to the corresponding baseline.

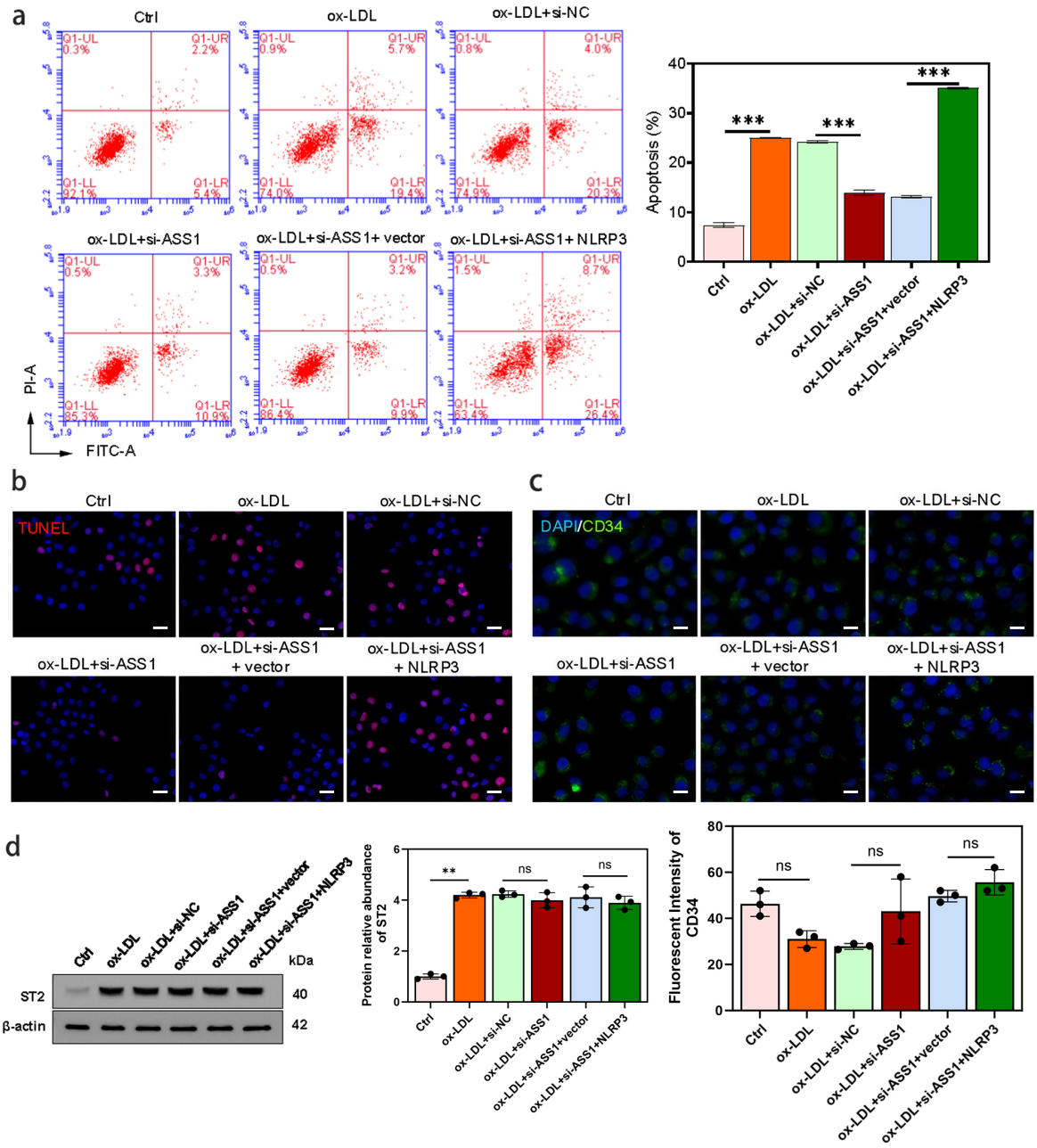

Fig. 8. NLRP3 overexpression in foam cells reverses the protective effects of ASS1 knockdown on HUVEC apoptosis. HUVECs were co-cultured with U937 foam cells from control, si-NC, si-ASS1, si-ASS1 + vector, and si-ASS1 + NLRP3 groups. (a) Flow cytometry assay to determine cell apoptotic rate. (b) TUNEL fluorescence FITC kit used to detect apoptotic endothelial cells. (c) Immunofluorescence staining of the vascular marker CD34. (d) Western blot analysis of ST2 protein levels. The scale bar is 50 µm in (b,c). For all panels, n = 3 biologically independent experiments (performed on different days with different HUVEC donors and different U937 passages); each experiment contained 3 technical replicates (wells) per group, with 1×10^5 HUVECs per well. Data are presented as mean ± standard deviation (SD). Error bars represent SD. $^{**}p < 0.01$, $^{***}p < 0.001$. ns, no significance (one-way ANOVA with repeated measures and Tukey post-hoc test relative to the corresponding baseline).

lated by ASS1 overexpression and downregulated by ASS1 knockdown (Fig. 10f), consistent with the *in vitro* findings.

ELISA of serum cytokines showed that IL-33 was elevated in AS mice, further increased by ASS1 overexpression, and attenuated by ASS1 knockdown (Fig. 10g). To determine whether NLRP3 activation also affects other inflammatory mediators, we measured IL-1β. Serum IL-1β was significantly higher in AS mice than in sham controls. ASS1 overexpression further raised IL-1β levels by ~1.7-fold relative to the NC group, while ASS1 knockdown reduced IL-1β by 42% ($p < 0.001$; Fig. 10h).

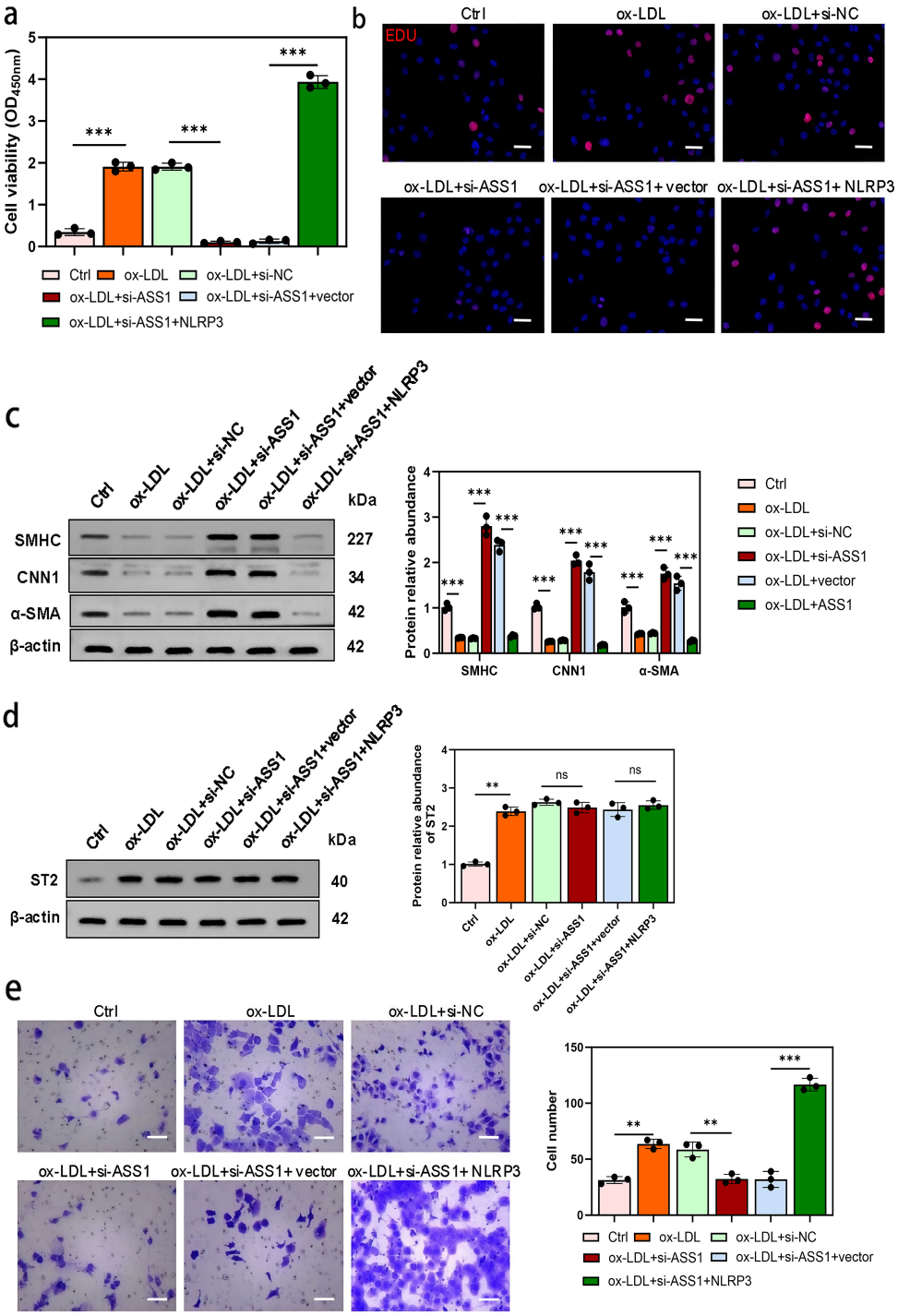

Fig. 9. NLRP3 overexpression in foam cells restores HAVSMC proliferation, migration, and dedifferentiation suppressed by ASS1 knockdown. HAVSMCs were co-cultured with U937 foam cells from control, si-NC, si-ASS1, si-ASS1 + vector, and si-ASS1 + NLRP3 groups. (a) Cell viability was assessed by the CCK-8 assay. (b) Cell proliferation of HAVSMCs was evaluated using EdU staining. (c) Western blot analysis of SMHC, CNN1, and α-SMA protein levels. (d) Western blot analysis of ST2 protein levels. (e) Transwell assay to determine cell migration in HAVSMCs. The scale bar is 50 µm in (b), and the scale bar is 100 µm in (e). For all panels, n = 3 biologically independent experiments (performed on different days with different HAVSMC lots and different U937 passages); each experiment contained 3 technical replicates (wells) per group, with 1×10^4 HAVSMCs per well for CCK-8, 2×10^4 HAVSMCs per well for EdU, 6-well plates for Western blot, and 24-well Transwell inserts for migration. Data are presented as mean $\pm$ standard deviation (SD). Error bars represent SD. ns, not significant ($p \geq 0.05$), **$p < 0.01$, ***$p < 0.001$ by one-way ANOVA with Tukey post-hoc test relative to the corresponding baseline.

These *in vivo* results demonstrate that ASS1 exacerbates plaque lipid deposition, activates the NLRP3 inflammasome and STAT3 signaling, and enhances the secretion of pro-inflammatory cytokines IL-33 and IL-1β, thereby promoting atherosclerotic progression.

4. Discussion

AS is a complex inflammatory disorder affecting medium and large arteries, primarily involving three key cell types: macrophages, endothelial cells, and smooth muscle cells [20,21]. In the initial stages of AS, the accumulation of oxidized low-density lipoprotein (ox-LDL) leads to macrophage dysfunction, resulting in the formation of foam cells and the production of pro-inflammatory cytokines [22]. Extensive research has established the crucial role of ASS1, a key enzyme in arginine biosynthesis, in regulating inflammatory macrophage activation and providing defense against bacterial infections by depleting cellular citrulline [15]. Zhang *et al*. [23] demonstrated that arginine can partially regulate the activation of the NLRP3 inflammasome by inhibiting ROS production in vascular endothelial cells. Building on these observations, we hypothesized that ASS1 is implicated in the regulation of pro-inflammatory cytokine production during foam cell formation. Our findings in this present study revealed that ox-LDL treatment significantly increased the production of reactive oxygen species (ROS) and upregulated the expression of argininosuccinate synthase 1 (ASS1) in PMA-induced macrophage-like U937 cells. Importantly, knocking down ASS1 notably reduced ox-LDL-induced ROS production and the secretion of interleukin-33 (IL-33), suggesting a positive regulatory role of ASS1 in IL-33 production in U937 foam cells.

Importantly, our rescue experiments using si-STAT3 and a constitutively active STAT3 mutant (STAT3-CA) provide direct evidence that STAT3 activation is a critical downstream event in ASS1-mediated pro-inflammatory signaling. The fact that STAT3 inhibition completely reversed the effects of ASS1 overexpression on NLRP3, adhesion molecules, ROS, and IL-33, while constitutive STAT3 activation restored the inflammatory phenotype suppressed by ASS1 knockdown, establishes a causal link between ASS1 and STAT3 phosphorylation. This moves beyond correlation and defines a clear signaling axis: ASS1 upregulation enhances STAT3 activation, which in turn drives NLRP3 inflammasome assembly and IL-33 secretion, thereby amplifying foam cell-driven inflammation in atherosclerosis. Furthermore, our study revealed that NLRP3 overexpression reversed the decrease in ROS production and IL-33 secretion induced by ASS1 silencing in U937 foam cells, which aligns with previous research indicating that the accumulation of ox-LDL enhances NLRP3 expression, leading to the assembly of the NLRP3 inflammasome complex in macrophages derived from THP-1 cells [24]. Notably, our rescue experiments with NLRP3 overexpression alone revealed that NLRP3 activation is sufficient to mimic the pro-inflammatory effects of ASS1 overexpression, including enhanced ROS production, upregulation of adhesion molecules, and elevated IL-33 secretion. Importantly, the effects of ASS1 knockdown were largely reversed by NLRP3 overexpression, suggesting that NLRP3 acts downstream of ASS1 and STAT3, and is a primary mediator of its pro-atherogenic functions. Collectively, these findings indicate that the ox-LDL-induced upregulation of ASS1 can activate the STAT3/NLRP3 inflammasome axis in U937 foam cells.

Endothelial cell injury is widely acknowledged as a critical and initiating factor in the development of AS [25]. In our co-culture system consisting of U937 foam cells and HUVECs, we observed that the knockdown of ASS1 in foam cells significantly inhibited ox-LDL-induced apoptosis. Moreover, our Western blot analysis revealed that ASS1 overexpression in foam cells significantly upregulated cleaved PARP and Bax expression while downregulating Bcl-2 in co-cultured HUVECs, resulting in an elevated Bax/Bcl-2 ratio. These findings suggest that ASS1 promotes HUVEC apoptosis through the mitochondrial pathway, further supporting the involvement of intrinsic apoptosis in ASS1-mediated endothelial injury during atherosclerosis.

ST2, also known as interleukin-1 receptor-like-1 protein (IL1RL1), is produced by T cells and endothelial cells [26] and has been shown to have significant involvement in cardiovascular diseases [27]. The IL-33/ST2 pathway, which is predominantly found in the endothelium of arterial vessels, is now recognized as a key player in the inflammatory mechanisms underlying AS [28]. The ST2 receptor has two isoforms: soluble decoy receptor (sST2) and membrane-bound signaling receptor (ST2L), which exert opposing biological effects. Their dynamic balance dictates disease outcome. ST2L mediates protection: IL-33 binding activates the MyD88/NF-κB pathway in endothelial cells, smooth muscle cells, regulatory T cells and macrophages, driving a Th2-polarized, anti-inflammatory response that promotes plaque stability and macrophage M2 polarization. In ApoE$^{-/-}$ mice, IL-33 administration or ST2L overexpression reduces plaque burden and increases stability. Conversely, sST2 acts destructively by sequestering IL-33, blocking its access to ST2L and thus abolishing protective signaling. Elevated sST2 favors pro-inflammatory Th1 responses, exacerbates inflammation, and destabilizes plaques. Clinically, plasma sST2 is an independent predictor of cardiovascular events and correlates with severe coronary artery disease and poor heart-failure outcomes.

Critically, our new data reveal that ASS1 does not uniformly increase total ST2, but specifically shifts the balance between its isoforms. ASS1 upregulation in foam cells promotes the expression of the soluble decoy receptor (sST2) while suppressing the membrane-bound signaling receptor

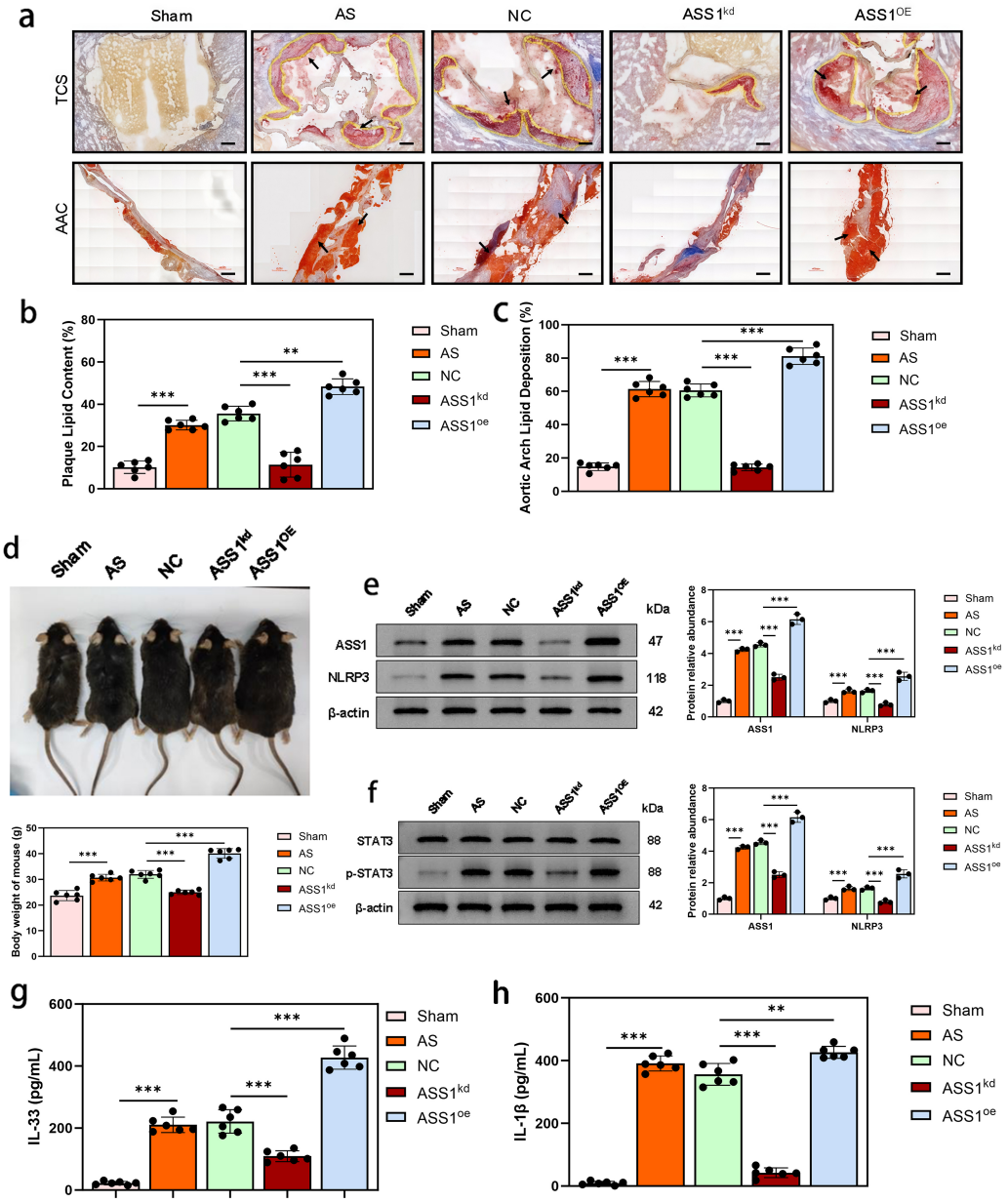

Fig. 10. ASS1 exacerbates atherosclerotic plaque progression, inflammation, and systemic metabolism in ApoE-deficient mice. Atherosclerosis was induced by feeding a high-fat diet for 12 weeks, followed by AAV9-mediated knockdown or overexpression of ASS1. Grouping: wild-type sham-operated group (Sham), atherosclerotic model group (AS), negative control group (NC, empty vector), ASS1 knockdown group ($ASS1^{kd}$), and ASS1 overexpression group ($ASS1^{OE}$). (a) Representative images of Oil Red O staining of the transverse cardiac section (TCS) and aortic arch cut (AAC). The black arrows in the figure indicate the severe areas of plaque lipid accumulation. (b,c) Quantification of lipid deposition of the TCS and AAC (Oil Red O-positive area percentage within plaque). (d) Body weight of mice measured at the study endpoint and comparative analysis between groups. (e) Western blot analysis (left) and quantitative summary (right) of ASS1 and NLRP3 protein expression in vascular tissues (n = 3 independent biological replicates). (f) Western blot analysis (left) and quantitative summary (right) of STAT3 and phosphorylated STAT3 (p-STAT3) protein levels in vascular tissues. (g,h) Serum IL-33 and serum IL-1β concentration measured by ELISA. The scale bar is 100 μm for TCS and 200 μm for AAC in (a). For all panels: n = 6 mice per group (exact number); each mouse represents one biological replicate. Animals were 8-week-old male $ApoE^{-/-}$ mice (C57BL/6 background), single-caged, fed a high-fat diet for 12 weeks, and injected with AAV9 on three separate days (3 independent cohorts) to ensure reproducibility. Tissue samples were collected once per mouse. Data presented are as mean ± standard deviation (SD). Error bars represent SD. $^{**}p < 0.01$, $^{***}p < 0.001$ compared to the control. Comparisons were made with 1-way ANOVA.

(ST2L) in both foam cells themselves and in co-cultured HUVECs/HAVSMCs. This shift results in an increased sST2/ST2L ratio. Emerging evidence supports the involvement of the IL-33/ST2 signaling pathway in the inflammatory pathogenesis of various injury-related diseases [29]. A recent investigation by Ma *et al.* [30] demonstrated that co-culturing NLRP3-overexpressing rat renal macrophages with NRK-52E cells led to NLRP3 activation in resident macrophages, resulting in the upregulation of IL-33. Subsequently, IL-33 mediated the IL-33/ST2/NF-κB pathway, promoting the inflammatory response of renal tubular epithelial cells. Based on our observations, we discovered that the increased expression of ASS1 in foam cells triggers the activation of the STAT3/NLRP3 inflammasome axis, leading to elevated IL-33 and ST2 (predominantly sST2) expression and secretion. Regarding HUVECs, the upregulated sST2 acts as a decoy receptor, preventing IL-33 from binding to ST2L on neighboring cells. This blockade of the IL-33/ST2L interaction inhibits the protective signaling that would otherwise reduce plaque burden and enhance plaque stability, thereby promoting endothelial cell damage and apoptosis [31]. This clarifies the precise mechanism by which ASS1 exacerbates inflammation via the IL-33/ST2 axis.

In addition to endothelial cells, abnormal proliferation, apoptosis, and migration of VSMCs have been strongly implicated in the progression of AS [32,33]. Ox-LDL, a significant contributor to AS progression, has been shown to impact VSMC apoptosis, proliferation, and migration [34]. In our study, we observed that ASS1 knockdown in foam cells significantly inhibited ox-LDL-induced proliferation and migration, as well as the expression of smooth muscle cell markers (SMHC, SNN1, and α-SMA) in HAVSMCs within the co-culture system with U937 foam cells. Importantly, these effects were reversed upon NLRP3 overexpression in foam cells. Increasing evidence suggests that foam cells can produce increased levels of inflammatory cytokines and growth factors, which act as stimulants, promoting the migration of quiescent VSMCs from the medial layer to the intima. This phenomenon triggers VSMC proliferation and enhances the synthesis of extracellular matrix proteins, ultimately leading to intimal thickening and subsequent blood vessel occlusion [35,36]. Given the substantial impact of NLRP3 inflammasome activation on atherogenesis, inflammation, and foam cell formation, its crucial role in triggering phenotypic transitions in VSMCs is widely acknowledged, contributing to plaque destabilization [37]. Based on these findings, it can be inferred that increased ASS1 expression in foam cells initiates the activation of the STAT3/NLRP3 inflammasome axis, leading to enhanced expression and release of IL-33 and ST2 (predominantly sST2). For HAVSMCs, sST2 acts as a decoy receptor, preventing IL-33 from binding to ST2L on smooth muscle cells. This blockade of the protective signaling normally mediated by IL-33/ST2L interaction induces a phenotypic switch in smooth muscle cells toward a proliferative state, characterized by aberrantly enhanced migratory capacity.

The role of ASS1 in atherosclerosis (AS) was further investigated using an ApoE-deficient mouse model fed a high-fat diet for 12 weeks. Modulation of ASS1 expression via AAV9 vectors demonstrated significant effects on lipid accumulation and inflammatory responses in AS mice. Oil Red O staining revealed that ASS1 knockdown reduced lipid accumulation in the hearts and aortas, while ASS1 overexpression exacerbated lipid enrichment compared to controls. These findings highlight ASS1 as a key regulator of lipid deposition in AS. In addition, ASS1 expression significantly influenced the levels of NLRP3 and p-STAT3 in vascular tissues, consistent with the regulation of inflammatory pathways observed *in vitro*. ASS1 knockdown decreased NLRP3 levels, whereas overexpression of ASS1 led to elevated NLRP3 expression. Similarly, p-STAT3 was downregulated with ASS1 knockdown but upregulated with ASS1 overexpression. Furthermore, ELISA assays showed that ASS1 regulated IL-33 levels in the serum of AS mice, with ASS1 overexpression increasing IL-33 concentration and knockdown reducing it. In addition to IL-33, our study also demonstrated that ASS1 overexpression significantly enhanced serum IL-1β levels in atherosclerotic mice, whereas ASS1 knockdown suppressed IL-1β secretion. This finding suggests that ASS1-mediated NLRP3 inflammasome activation is not limited to the IL-33/ST2 axis but also involves the release of other pro-inflammatory cytokines such as IL-1β. These results further support the role of ASS1 as a broad regulator of inflammasome activity in atherosclerosis, contributing to a more comprehensive inflammatory milieu that exacerbates plaque progression. Overall, these results confirm that ASS1 modulates lipid accumulation and inflammation in AS through mechanisms involving the STAT3/NLRP3 axis and downstream cytokines, including IL-33 and IL-1β.

Based on our results, a pattern of ASS1-mediated NLRP3/IL-33/ST2 pathway on inflammatory responses in foam cells during atherosclerosis was proposed (Fig. 11). Upon excessive levels of oxidative stress in in blood vessels, ox-LDL enter the macrophage through receptor-mediated endocytosis, which results in the pro-inflammatory polarization of the macrophage and leads to the activation of JAK2-STAT1 signaling pathway that upregulates intracellular ASS1. This mechanism of ox-LDL-induced ASS1 elevation has been validated in the study by Mao *et al.* [15]. and further verified in our present study. Elevated intracellular ASS1 induces the phosphorylation of STAT3. Subsequently, p-STAT3 translocates from the cytoplasm to the nucleoplasm and then stimulates gene expression through binding of p-STAT3 to a conserved DNA element gamma-activated sequence (GAS), initiating NLRP3-related gene transcription. The activation of the NLRP3 inflammasome leads to increased expression and

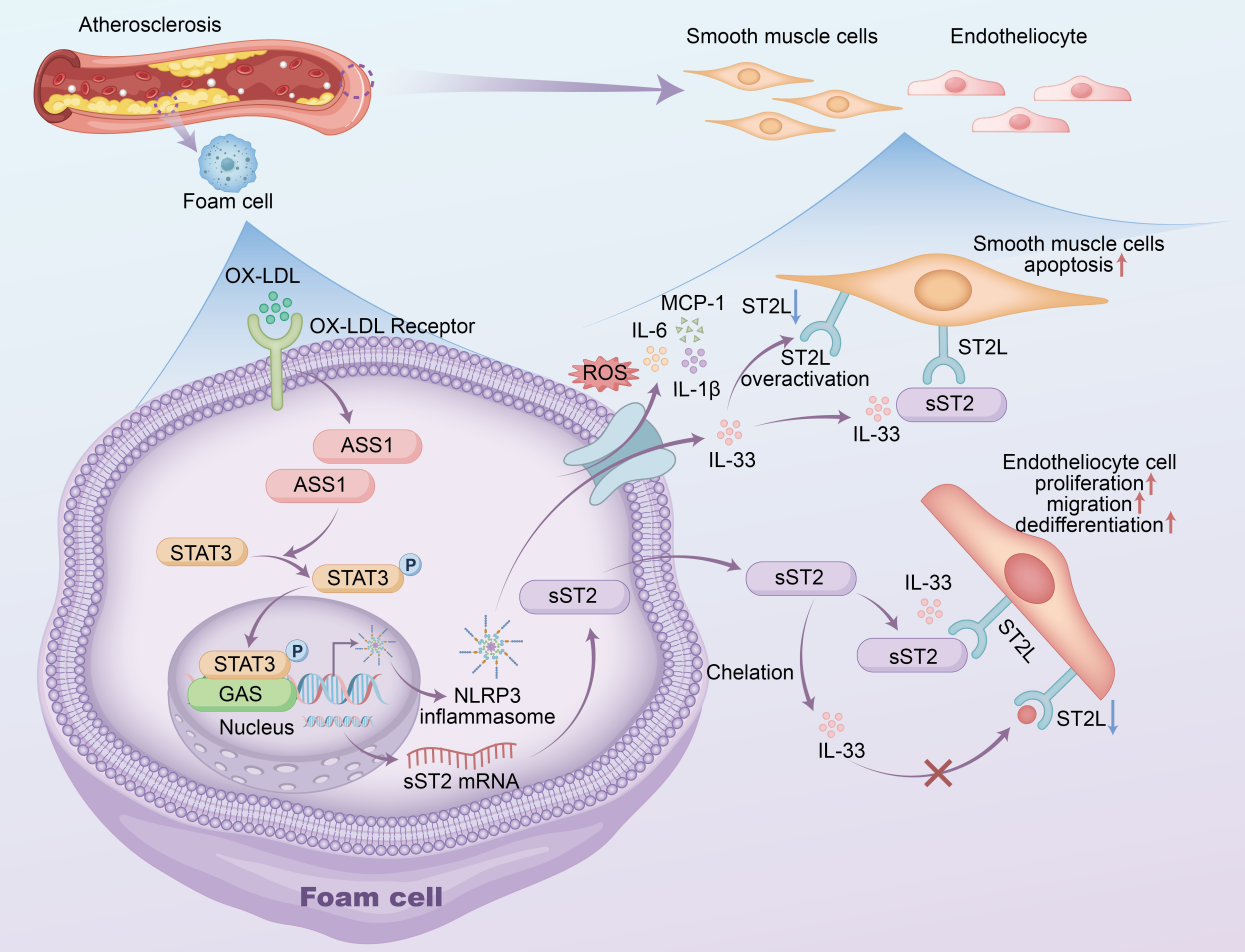

Fig. 11. A pattern of ASS1-mediated NLRP3/IL-33/ST2 pathway on inflammatory responses in foam cells during atherosclerosis was proposed. A pattern of ASS1-mediated NLRP3/IL-33/ST2 pathway on inflammatory responses in foam cells during atherosclerosis was proposed. Our findings delineate a coherent pro-inflammatory signaling cascade in atherosclerosis: ox-LDL $\rightarrow$ ASS1 $\uparrow$ $\rightarrow$ p-STAT3 $\uparrow$ $\rightarrow$ NLRP3 Inflammasome Activation $\rightarrow$ IL-33/IL-1β Secretion $\uparrow$ + ST2 Isoform Shift (sST2 $\uparrow$/ST2L $\downarrow$) $\rightarrow$ Elevated sST2 blocks IL-33 binding to ST2L through sequestration $\rightarrow$ Endothelial Apoptosis & VSMC Phenotypic Modulation $\rightarrow$ Atherosclerosis Progression. This pathway integrates ASS1's regulation of both cytokine production and receptor bioavailability, providing a more comprehensive mechanistic understanding of its pro-atherogenic role. The up arrows ($\uparrow$) indicate upregulation, and the down arrows ($\downarrow$) indicate downregulation.

secretion of IL-33 (and IL-1β). Critically, we found that ASS1 upregulation disrupts ST2 receptor balance by elevating sST2 and suppressing ST2L. ASS1/STAT3/NLRP3 axis activation drives foam cells to overproduce and secrete sST2, elevating its local and systemic levels. This upregulated sST2 sequesters IL-33, blocking its binding to ST2L on neighboring cells and thereby inhibiting the plaque-stabilizing, protective IL-33/ST2L signaling. Consequently, endothelial apoptosis and smooth muscle cell phenotypic switching/migration are promoted, establishing a self-amplifying inflammatory loop: inflammation $\rightarrow$ IL-33 overproduction $\rightarrow$ sST2 release $\rightarrow$ protection blockade $\rightarrow$ exacerbated inflammation. The concurrent ST2L downregulation may stem from either ligand-induced internalization/degradation due to excessive IL-33-driven ST2L overactivation, or transcriptional downregulation resulting from prolonged ligand deprivation caused by sST2-mediated IL-33 sequestration. These possibilities require further experimental validation.

5. Limitations

Several limitations warrant mention. First, while we establish STAT3 as a key downstream effector of ASS1, emerging data show that JAK2-STAT1 signaling upregulates ASS1 [15], raising the possibility of a reciprocal ASS1/STAT1 axis that may independently modulate atherosclerosis, which was not examined here. Second, modulating ASS1 could influence foam-cell formation efficiency under ox-LDL stimulation, potentially confounding inflammatory readouts due to variations in foam-cell number or lipid-loading state across groups. Third, although

we propose a self-amplifying loop where ASS1-driven IL-33/sST2 elevation blocks protective ST2L signaling, the mechanism for concurrent ST2L downregulation—whether through ligand-induced internalization or transcriptional suppression—remains speculative and needs experimental validation. Finally, our focus on the NLRP3/IL-33/ST2 axis does not exclude roles for other NLRP3-dependent cytokines (e.g., IL-1β) in ASS1-mediated atherogenesis, whose relative contributions require further study.

6. Conclusions

In summary, this study identifies argininosuccinate synthase 1 (ASS1) as a critical regulator of atherosclerotic inflammation via the STAT3/NLRP3/IL-33/ST2 signaling axis. We show that oxidized low-density lipoprotein (ox-LDL) upregulates ASS1 expression in macrophage-derived foam cells, which in turn activates NLRP3 inflammasome assembly in a STAT3-dependent manner and enhances the secretion of pro-inflammatory cytokines IL-33 and IL-1β. Moreover, ASS1 promotes a shift in the ST2 receptor balance toward the soluble decoy isoform sST2, thereby impairing the protective IL-33/ST2L signaling axis. Functionally, ASS1 drives endothelial cell apoptosis through the mitochondrial pathway and facilitates vascular smooth muscle cell proliferation, migration, and phenotypic switching. *In vivo*, modulation of ASS1 expression significantly affects atherosclerotic plaque lipid accumulation and systemic inflammatory responses. Collectively, these results position ASS1 as a central integrator of foam cell-mediated vascular inflammation and underscore its potential as a therapeutic target in atherosclerosis.

Availability of Data and Materials

The data used to support the findings of this study are available from the corresponding author Dr. Kefei Dou upon reasonable request. The data are not publicly available due to privacy or ethical restrictions.

Author Contributions

All authors have participated sufficiently in the work and agreed to be accountable for all aspects of the work. KD had full access to all of the data in the study and takes responsibility for the integrity of the data and the accuracy of the data analysis. KD and DM contributed to the conception and design of the work. SW and FH performed the cytology experiments and gene expression analysis. ZQ, SY, and XB established the animal model and performed the statistical analysis. BZ participated in data interpretation and the preparation of figures/tables. SW and FH drafted the manuscript. KD, DM, and BZ critically revised the manuscript. KD and DM finalized the manuscript. All authors contributed to editorial changes in the manuscript. All the authors reviewed and approved the final version.

Ethics Approval and Consent to Participate

The experimental protocol was reviewed and approved by the Institutional Animal Care and Use Committee of Peking Union Medical College (PUMC). All animal procedures were conducted in strict accordance with the guidelines and regulations for the care and use of laboratory animals, and adhered to the principles of the 3Rs (Replacement, Reduction, and Refinement) to minimize animal suffering and distress. The formal ethical approval document was subsequently issued by Fuwai Hospital, an affiliate of the Chinese Academy of Medical Sciences (CAMS) and a constituent of PUMC. A scanned copy of the official ethical approval document is available for submission upon request (Approval No. 0105-1-6-ZX(X)-4).

Acknowledgment

Not applicable.

Funding

The research reported in this publication was supported by the Noncommunicable Chronic Diseases-National Science and Technology Major Project (grant number 2025ZD0548200).

Conflict of Interest

The authors declare no conflict of interest.

Supplementary Material

Supplementary material associated with this article can be found, in the online version, at https://doi.org/10.31083/FBL47686.

References

[1] Hilgendorf I, Swirski FK, Robbins CS. Monocyte fate in atherosclerosis. Arteriosclerosis, Thrombosis, and Vascular Biology. 2015; 35: 272–279. https://doi.org/10.1161/ATVBAHA.114.303565.

[2] Rafieian-Kopaei M, Setorki M, Doudi M, Baradaran A, Nasri H. Atherosclerosis: process, indicators, risk factors and new hopes. International Journal of Preventive Medicine. 2014; 5: 927–946.

[3] Yu XH, Fu YC, Zhang DW, Yin K, Tang CK. Foam cells in atherosclerosis. Clinica Chimica Acta; International Journal of Clinical Chemistry. 2013; 424: 245–252. https://doi.org/10.1016/j.cca.2013.06.006.

[4] Ooi BK, Goh BH, Yap WH. Oxidative Stress in Cardiovascular Diseases: Involvement of Nrf2 Antioxidant Redox Signaling in Macrophage Foam Cells Formation. International Journal of Molecular Sciences. 2017; 18: 2336. https://doi.org/10.3390/ijms18112336.

[5] Chinetti-Gbaguidi G, Colin S, Staels B. Macrophage subsets in atherosclerosis. Nature Reviews. Cardiology. 2015; 12: 10–17. https://doi.org/10.1038/nrcardio.2014.173.

[6] Truong R, Thankam FG, Agrawal DK. Immunological mechanisms underlying sterile inflammation in the pathogenesis of atherosclerosis: potential sites for intervention. Expert Review of Clinical Immunology. 2021; 17: 37–50. https://doi.org/10.1080/1744666X.2020.1860757.

[7] Grebe A, Hoss F, Latz E. NLRP3 Inflammasome and the IL-1 Pathway in Atherosclerosis. Circulation Research. 2018;

122: 1722–1740. https://doi.org/10.1161/CIRCRESAHA.118.311362.

[8] Westerterp M, Fotakis P, Ouimet M, Bochem AE, Zhang H, Molusky MM, *et al*. Cholesterol Efflux Pathways Suppress Inflammasome Activation, NETosis, and Atherogenesis. Circulation. 2018; 138: 898–912. https://doi.org/10.1161/CIRCULATIONAHA.117.032636.

[9] Zhang J, Chen Z, Ma M, He Y. Soluble ST2 in coronary artery disease: Clinical biomarkers and treatment guidance. Frontiers in Cardiovascular Medicine. 2022; 9: 924461. https://doi.org/10.3389/fcvm.2022.924461.

[10] McLaren JE, Michael DR, Salter RC, Ashlin TG, Calder CJ, Miller AM, *et al*. IL-33 reduces macrophage foam cell formation. Journal of Immunology (Baltimore, Md.: 1950). 2010; 185: 1222–1229. https://doi.org/10.4049/jimmunol.1000520.

[11] Zhuang T, Liu J, Chen X, Zhang L, Pi J, Sun H, *et al*. Endothelial Foxp1 Suppresses Atherosclerosis via Modulation of Nlrp3 Inflammasome Activation. Circulation Research. 2019; 125: 590–605. https://doi.org/10.1161/CIRCRESAHA.118.314402.

[12] Miller AM, Liew FY. The IL-33/ST2 pathway–A new therapeutic target in cardiovascular disease. Pharmacology & Therapeutics. 2011; 131: 179–186. https://doi.org/10.1016/j.pharmthera.2011.02.005.

[13] Tseng CCS, Huibers MMH, van Kuik J, de Weger RA, Vink A, de Jonge N. The Interleukin-33/ST2 Pathway Is Expressed in the Failing Human Heart and Associated with Pro-fibrotic Remodeling of the Myocardium. Journal of Cardiovascular Translational Research. 2018; 11: 15–21. https://doi.org/10.1007/s12265-017-9775-8.

[14] Thanikachalam PV, Ramamurthy S, Mallapu P, Varma SR, Narayanan J, Abourehab MA, *et al*. Modulation of IL-33/ST2 signaling as a potential new therapeutic target for cardiovascular diseases. Cytokine & Growth Factor Reviews. 2023; 71-72: 94–104. https://doi.org/10.1016/j.cytogfr.2023.06.003.

[15] Mao Y, Shi D, Li G, Jiang P. Citrulline depletion by ASS1 is required for proinflammatory macrophage activation and immune responses. Molecular Cell. 2022; 82: 527–541.e7. https://doi.org/10.1016/j.molcel.2021.12.006.

[16] Jeyabalan G, Klune JR, Nakao A, Martik N, Wu G, Tsung A, *et al*. Arginase blockade protects against hepatic damage in warm ischemia-reperfusion. Nitric Oxide: Biology and Chemistry. 2008; 19: 29–35. https://doi.org/10.1016/j.niox.2008.04.002.

[17] Liu Q, Shang Y, Tao Z, Li X, Shen L, Zhang H, *et al*. Coxsackievirus group B3 regulates ASS1-mediated metabolic reprogramming and promotes macrophage inflammatory polarization in viral myocarditis. Journal of Virology. 2024; 98: e0080524. https://doi.org/10.1128/jvi.00805-24.

[18] Ryoo S, Gupta G, Benjo A, Lim HK, Camara A, Sikka G, *et al*. Endothelial arginase II: a novel target for the treatment of atherosclerosis. Circulation Research. 2008; 102: 923–932. https://doi.org/10.1161/CIRCRESAHA.107.169573.

[19] Zuo Q, Zhang G, He L, Ma S, Ma H, Zhai J, *et al*. Canagliflozin Attenuates Hepatic Steatosis and Atherosclerosis Progression in Western Diet-Fed ApoE-Knockout Mice. Drug Design, Development and Therapy. 2022; 16: 4161–4177. https://doi.org/10.2147/DDDT.S388823.

[20] Reglero-Real N, Colom B, Bodkin JV, Nourshargh S. Endothelial Cell Junctional Adhesion Molecules: Role and Regulation of Expression in Inflammation. Arteriosclerosis, Thrombosis, and Vascular Biology. 2016; 36: 2048–2057. https://doi.org/10.1161/ATVBAHA.116.307610.

[21] Liu C, Wu J, Jia H, Lu C, Liu J, Li Y, *et al*. Oncostatin M promotes the ox-LDL-induced activation of NLRP3 inflammasomes via the NF-κB pathway in THP-1 macrophages and promotes the progression of atherosclerosis. Annals of Translational Medicine. 2022; 10: 456. https://doi.org/10.21037/atm-22-560.

[22] Oppi S, Nusser-Stein S, Blyszczuk P, Wang X, Jomard A, Marzolla V, *et al*. Macrophage NCOR1 protects from atherosclerosis by repressing a pro-atherogenic PPARγ signature. European Heart Journal. 2020; 41: 995–1005. https://doi.org/10.1093/eurheartj/ehz667.

[23] Zhang M, Li Y, Guo Y, Xu J. Arginine Regulates NLRP3 Inflammasome Activation Through SIRT1 in Vascular Endothelial Cells. Inflammation. 2021; 44: 1370–1380. https://doi.org/10.1007/s10753-021-01422-1.

[24] Zeng W, Wu D, Sun Y, Suo Y, Yu Q, Zeng M, *et al*. The selective NLRP3 inhibitor MCC950 hinders atherosclerosis development by attenuating inflammation and pyroptosis in macrophages. Scientific Reports. 2021; 11: 19305. https://doi.org/10.1038/s41598-021-98437-3.

[25] Młynarska E, Bojdo K, Frankenstein H, Krawiranda K, Kustosik N, Lisińska W, *et al*. Endothelial Dysfunction as the Common Pathway Linking Obesity, Hypertension and Atherosclerosis. International Journal of Molecular Sciences. 2025; 26: 10096. https://doi.org/10.3390/ijms262010096.

[26] Houghton-Triviño N, Salgado DM, Rodríguez JA, Bosch I, Castellanos JE. Levels of soluble ST2 in serum associated with severity of dengue due to tumour necrosis factor alpha stimulation. The Journal of General Virology. 2010; 91: 697–706. https://doi.org/10.1099/vir.0.012971-0.

[27] McCarthy CP, Januzzi JL, Jr. Soluble ST2 in Heart Failure. Heart Failure Clinics. 2018; 14: 41–48. https://doi.org/10.1016/j.hfc.2017.08.005.

[28] Aimo A, Migliorini P, Vergaro G, Franzini M, Passino C, Maisel A, *et al*. The IL-33/ST2 pathway, inflammation and atherosclerosis: Trigger and target? International Journal of Cardiology. 2018; 267: 188–192. https://doi.org/10.1016/j.ijcard.2018.05.056.

[29] Chen WY, Li LC, Yang JL. Emerging Roles of IL-33/ST2 Axis in Renal Diseases. International Journal of Molecular Sciences. 2017; 18: 783. https://doi.org/10.3390/ijms18040783.

[30] Ma Q, Xu M, Jing X, Qiu J, Huang S, Yan H, *et al*. Honokiol suppresses the aberrant interactions between renal resident macrophages and tubular epithelial cells in lupus nephritis through the NLRP3/IL-33/ST2 axis. Cell Death & Disease. 2023; 14: 174. https://doi.org/10.1038/s41419-023-05680-9.

[31] Bayés-Genís A, Núñez J, Lupón J. Soluble ST2 for Prognosis and Monitoring in Heart Failure: The New Gold Standard? Journal of the American College of Cardiology. 2017; 70: 2389–2392. https://doi.org/10.1016/j.jacc.2017.09.031.

[32] Doran AC, Meller N, McNamara CA. Role of smooth muscle cells in the initiation and early progression of atherosclerosis. Arteriosclerosis, Thrombosis, and Vascular Biology. 2008; 28: 812–819. https://doi.org/10.1161/ATVBAHA.107.159327.

[33] Wang P, Xu TY, Guan YF, Zhao Y, Li ZY, Lan XH, *et al*. Vascular smooth muscle cell apoptosis is an early trigger for hypothyroid atherosclerosis. Cardiovascular Research. 2014; 102: 448–459. https://doi.org/10.1093/cvr/cvu056.

[34] Pirillo A, Norata GD, Catapano AL. LOX-1, OxLDL, and atherosclerosis. Mediators of Inflammation. 2013; 2013: 152786. https://doi.org/10.1155/2013/152786.

[35] Kriszbacher I, Koppán M, Bódis J. Inflammation, atherosclerosis, and coronary artery disease. The New England Journal of Medicine. 2005; 353: 429–430; author reply 429–430.

[36] Bentzon JF, Otsuka F, Virmani R, Falk E. Mechanisms of plaque formation and rupture. Circulation Research. 2014; 114: 1852–1866. https://doi.org/10.1161/CIRCRESAHA.114.302721.

[37] Burger F, Baptista D, Roth A, da Silva RF, Montecucco F, Mach F, *et al*. NLRP3 Inflammasome Activation Controls Vascular Smooth Muscle Cells Phenotypic Switch in Atherosclerosis. International Journal of Molecular Sciences. 2021; 23: 340. https://doi.org/10.3390/ijms23010340.